HHS Public Access

Author manuscript

Cancer Cell. Author manuscript; available in PMC 2024 June 07.

Published in final edited form as:

Cancer Cell. 2023 July 10; 41(7): 1363–1380.e7. doi:10.1016/j.ccell.2023.05.015.

MCT4-dependent lactate secretion suppresses antitumor immunity in LKB1-deficient lung adenocarcinoma

Yu Qian[1], **Ana Galan-Cobo**[1], **Irene Guijarro**[1], **Minghao Dang**[2], **David Molkentine**[1], **Alissa Poteete**[1], **Fahao Zhang**[1], **Qi Wang**[3], **Jing Wang**[3], **Edwin Parra**[4], **Apekshya Panda**[5], **Jacy Fang**[5,6], **Ferdinandos Skoulidis**[1], **Ignacio I. Wistuba**[4], **Svena Verma**[7], **Taha Merghoub**[7], **Jedd D. Wolchok**[7], **Kwok-Kin Wong**[8], **Ralph J. DeBerardinis**[9], **John D. Minna**[10], **Natalie I. Vokes**[1], **Catherine B. Meador**[11,12], **Justin F. Gainor**[6,12], **Linghua Wang**[2], **Alexandre Reuben**[1], **John V. Heymach**[1,13,*]

[1]Department of Thoracic/Head and Neck Medical Oncology, Houston, TX, USA

[2]Department of Genomic Medicine, Houston, TX, USA

[3]Department of Bioinformatics and Computational Biology, Houston, TX, USA

[4]Department of Translational Molecular Pathology, The University of Texas MD Anderson Cancer Center, Houston, TX, USA

[5]Broad Institute of MIT and Harvard, Cambridge, MA, USA

[6]Center for Cancer Research, Department of Medicine, Massachusetts General Hospital, Boston, MA, USA

[7]Ludwig Collaborative and Swim Across America Laboratory, MSK, New York, NY, USA

[8]Division of Hematology & Medical Oncology, Laura and Isaac Perlmutter Cancer Center, New York University Langone Medical Center, New York, NY, USA

[9]Children's Medical Center Research Institute, University of Texas Southwestern Medical Center, Dallas, TX, USA

[10]Hamon Center for Therapeutic Oncology Research, UT Southwestern Medical Center, Dallas, TX, USA

[11]Department of Medicine, Division of Hematology/Oncology, Massachusetts General Hospital Cancer Center, Boston, MA, USA

[*]Correspondence: jheymach@mdanderson.org.

AUTHOR CONTRIBUTIONS

Conceptualization, Y.Q., A.G., and J.V.H.; Methodology, Y.Q., I.G., M.D., J.W., S.V., L.W., and J.F.G.; Investigation, Y.Q., I.G., M.D., D.M., A.P., F.Z., Q.W., A.P., and J.F.; Resources, A.P., E.P., F.S., I.I.W. T.M., J.D.W., K.K.W., R.J.D., J.D.M., N.I.V, C.B.M., J.F.G., and A.R.; Writing-Original Draft, Y.Q.; Writing-Review & Editing, A.G., I.G., R.J.D., J.D.M., A.R., and J.V.H; Supervision, J.V.H; Founding Acquisition, J.V.H.

DECLARATION OF INTERESTS

The other authors declare no competing interests.

INCLUSION AND DIVERSITY

We support inclusive, diverse, and equitable conduct of research.

SUPPLEMENTAL INFORMATION

Supplemental information can be found online at https://doi.org/10.1016/j.ccell.2023.05.015.

[12]Center for Thoracic Cancers, Massachusetts General Hospital, Boston, MA, USA

[13]Lead contact

SUMMARY

Inactivating *STK11*/LKB1 mutations are genomic drivers of primary resistance to immunotherapy in KRAS-mutated lung adenocarcinoma (LUAD), although the underlying mechanisms remain unelucidated. We find that LKB1 loss results in enhanced lactate production and secretion via the MCT4 transporter. Single-cell RNA profiling of murine models indicates that LKB1-deficient tumors have increased M2 macrophage polarization and hypofunctional T cells, effects that could be recapitulated by the addition of exogenous lactate and abrogated by MCT4 knockdown or therapeutic blockade of the lactate receptor GPR81 expressed on immune cells. Furthermore, MCT4 knockout reverses the resistance to PD-1 blockade induced by LKB1 loss in syngeneic murine models. Finally, tumors from *STK11*/LKB1 mutant LUAD patients demonstrate a similar phenotype of enhanced M2-macrophages polarization and hypofunctional T cells. These data provide evidence that lactate suppresses antitumor immunity and therapeutic targeting of this pathway is a promising strategy to reversing immunotherapy resistance in *STK11*/LKB1 mutant LUAD.

In brief

Qian et al. uncover that enhanced lactate secretion plays a critical role in promoting the immunotherapy-resistant phenotype observed in *STK11*/LKB1 mutant lung adenocarcinoma (LUAD). They demonstrate that increased lactate secretion via the MCT4 lactate transporter promotes M2 macrophage polarization and suppresses T cell function, and that targeting MCT4 improves the response to immune checkpoint blockade in tumors with *STK11*/LKB1 mutations.

Graphical Abstract

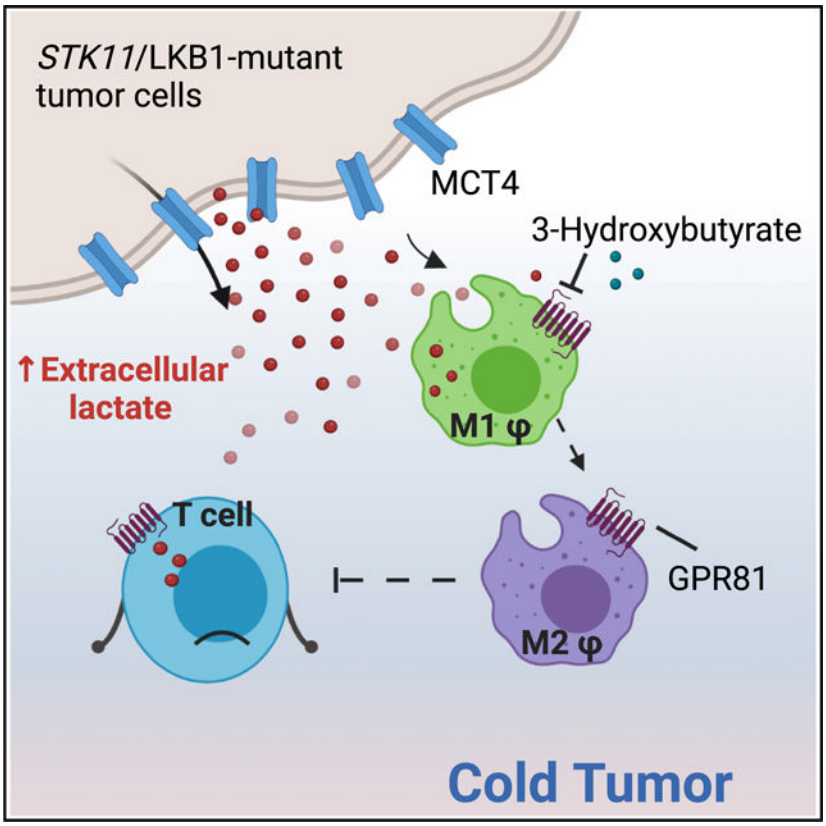

INTRODUCTION

Loss or inactivating mutations of the tumor suppressor gene serine/threonine kinase *STK11* encoding the LKB1 protein (henceforth referred to as *STK11*/LKB1 mutations) occurs in approximately 20% of lung adenocarcinoma (LUAD) and 2–19% of squamous cell carcinoma.[1–4] *STK11*/LKB1 is frequently co-mutated with *KRAS* (KL tumors), and these co-occurring alterations lead to a specific biological signature associated with a more aggressive phenotype.[5–8] While immunotherapy checkpoint blockade (ICB) has transformed the standard of care for cancer patients and is widely indicated to treat various malignancies, KL tumors are associated with resistance to immunotherapy, which has been shown to be effective against LKB1-proficient non-small cell lung cancer (NSCLC) tumors with *KRAS* mutation (K) or NSCLC tumors with *KRAS* and *TP53* comutations (KP).[9–11] Indeed, LKB1 loss has emerged as a major driver of a cold tumor immune-microenvironment (TIME), associated with low T cell infiltration, low PD-L1 expression, and enhanced recruitment of neutrophils and myeloid-derived suppressor cells (MDSCs).[12] In preclinical models, LKB1 deficiency has been shown to result in secretion of immunosuppressive chemokines and cytokines such as VEGF, IL-6, TGF-β, and CXCR2 ligands.[13,14]

LKB1 is a primary regulator of the 14 AMPK-related kinases.[15,16] More recently, the salt-inducible kinases (SIKs) have been identified as key substrates of LKB1 that suppress lung tumor formation and regulate gene expression.[17,18] Importantly, LKB1 loss has been associated with metabolic reprogramming, and synergizes with *KRAS* mutations to activate

hypoxia, glycolysis, and glutamine and serine metabolism,[19–21] through upregulation of pivotal genes such as HIF-1α or KEAP1-NRF2. Additionally, KL tumor cells overexpress the urea cycle enzyme carbamoyl phosphate synthetase-1 (CPS1), leading to nitrogen flow into pyrimidines to support cell growth.[22] The impact of the altered metabolic phenotype of KL tumors on the TIME is poorly understood and likely contributes to the immunosuppressive phenotype observed in these tumors.

Monocarboxylate transporter 4 (MCT4, also known as solute carrier family 16 member 3 or *SLC16A3*), is upregulated in hypoxia by HIF-1α, and is thought to be the primary mediator of lactic acid transportation across the plasma membrane which is fundamental for maintaining the flow of glycolysis.[23] MCT4 is overexpressed in several types of cancers, including NSCLC, and serves as an independent negative prognostic factor.[24] However, the impact of enhanced lactate production and MCT4-mediated lactate secretion on tumor progression and on the TIME, or more specifically in KL tumors, is unknown.

Here, we investigate the biological consequence of LKB1 loss on tumor immune-infiltration and lack of response to ICB. We establish that LKB1 loss significantly affects tumor metabolism by enhancing glycolysis as well as lactate production and secretion, effects that are dependent on the upregulation of the lactate transporter MCT4. We show that LKB1-deficient tumors display a reduced immune infiltration of $CD8^+$ T cells, but enhanced M2 macrophage polarization. Our findings indicate that enhanced lactate secretion in LKB1-deficient tumors contribute to M2 macrophage polarization and knock out of MCT4 partially depleted pro-tumoral M2 macrophages as well as enhanced ICB anti-tumor therapeutic response *in vivo*. Collectively, our data suggest that inhibition of MCT4 is a promising therapeutic strategy to overcome the inert TIME observed in LKB1-deficient tumors and potentially increase the clinical efficacy of immune checkpoint blockade in this patient population.

RESULTS

LKB1 deficiency increases lactate secretion

To further understand the impact of LKB1 deficiency, we performed single-cell RNA sequencing (scRNA-seq) analysis of murine *Kras*-mutant (LKR13 K) and *Kras*-mutant/LKB1-loss (LKR13 KL) syngeneic tumor models. LKB1-deficient tumors were reported to show an enhanced rate of glycolysis.[19] Consistent with this, gene set variation analysis (GSVA) on these tumor populations revealed a strong enrichment of genes related to glycolysis, as well as E2F signature and angiogenesis in KL compared to K tumors (Figure S1A). Subsequent studies were performed using isogenic pairs (+/− LKB1 expression) in our murine syngeneic LKR13/LKR10 and human (A549, H460, H23, and H2030) LUAD models. Restoring LKB1 expression significantly decreased extracellular acidification rate (ECAR) and increased oxygen consumption rate (OCR) (Figures 1A and 1B), while knockdown of LKB1 decreased OCR (Figure S1B). However, using 5-aminoimidazole-4-carboxamide riboside (AICAR) to activate AMPK, a key metabolic regulator downstream of LKB1, showed a reduction on both OCR and ECAR in LKB1 deficient cells, suggesting the metabolic alteration was not fully AMPK dependent (Figure S1C).

We next evaluated the impact of LKB1 deficiency on lactate production in LUAD tumor cells. The results from a prior study[22] and Cancer Cell Line Encyclopedia (CCLE) metabolomic profiling suggested that lactate levels were elevated in LKB1-deficient tumor samples and cell lines (Figures S1D and S1E). Moreover, we found that LKB1-deficient tumor cells produced higher extracellular lactate levels than their LKB1-proficient isogenic counterparts, while knockdown of LKB1 in H441 LKB1-proficient cells significantly increased lactate secretion (Figures 1C and 1D). Additionally, LKB1 loss significantly decreased intracellular pH (Figure 1E).

LKB1 loss upregulates MCT4 expression in LUAD tumor cells

MCT4 plays a key role in the transport of lactate and is upregulated in LUAD tumors compared to normal tissue (Figure S1F). Because of this, we sought to determine whether LKB1 modulates MCT4 expression. We observed varying expression levels of MCT4 across a panel of KL and KP cell lines (Figure S1G). More importantly, re-expressing LKB1, but not kinase-dead LKB1, in LKB1 deficient cell lines decreased MCT4 expression (Figures 1F–1G, S1H). Likewise, we found that the knockdown of LKB1 in KP cell line H2009 increased MCT4 expression, but not in H358 which harbors a mitochondrial NADH dehydrogenase mutation[25] (Figure S1I). Similar findings were observed in LKR13 and LKR10 murine models which also showed MCT4 was increased in LKB1 loss tumor cells (Figure 1H). Additionally, protein expression data from reverse phase proteomic arrays (RPPA) was consistent in that MCT4 expression is significantly upregulated in LKR13KL cells (Figure S1J). From the Cancer Genome Atlas (TCGA) cohort, we also observed a significant upregulation in MCT4 mRNA expression in LKB1 mutant tumors (Figure S1K). Moreover, cell surface MCT4 expression was also increased when evaluated by flow cytometry in both human and murine isogenic pair cell lines (Figure 1I). To investigate MCT4 expression in LKB1-proficient and -deficient tumors *in vivo*, we evaluated MCT4 expression in tumor tissues from K and KL genetically engineered mouse models (GEMMs) and syngeneic tumor models. Immunostaining showed a significantly increased level of MCT4 in KL tumors (Figures 1J and S1L).

Knockout of MCT4 impairs lactate secretion and cell viability in LKB1-deficient cells

To explore the functional role of MCT4 on cell growth and metabolism in LKB1-deficient tumors, we used CRISPR/Cas9 gene editing to knockout the MCT4 gene (MCT4-KO) in LKR13, LKR10 K, and KL cell lines. MCT4 loss reduced cell viability in both K and KL cells (Figures 2A, 2B, and S2A), although KL cells were impacted to a lesser extent. Consistent with its role in lactate transport, MCT4 depletion resulted in decreased levels of extracellular lactate and increased intracellular accumulation of lactate (Figures 2C and S2B). We assessed intracellular pH following MCT4 KO by immunofluorescence and flow cytometry and found that intracellular pH was significantly lower in MCT4-KO (Figures 2D and 2E). Furthermore, MCT4 loss led to a significantly decreased glycolytic and oxidative phosphorylation (OXPHOS) rate as assessed by ECAR and OCR quantification (Figures 2F and S2C). To further evaluate whether cellular energy production is dependent on MCT4, we converted ECAR and OCR measurements into ATP production rate as previously described.[26] The maximal glycolytic capacity of K and KL tumor cells was similar. However, KL cells displayed a significantly lower potential for mitochondrial respiration

compared to parental K cells (rectangle indicates maximum bioenergetic potential, Figure S2D). ATP production from glycolysis (J_{ATP} gly) and OxPhos (J_{ATP} oxphos) were similar in K, but not KL cells, consistent with the findings that KL cells are more dependent on glycolysis. As expected, MCT4 knockout dramatically impaired ATP production from both glycolysis and OxPhos (Figure S2E), as well as the maximal production capacity (Figures S2F and S2G). Collectively, these results indicate that LKB1 loss enhances MCT4 expression which promotes cell viability, ATP production, and extracellular lactate accumulation and acidification.

MCT4 knockout abrogates M2 macrophage polarization induced in LKB1-deficient tumors

Given that lactate is known to impact different cell types within the tumor microenvironment, we next asked whether the metabolic reprogramming associated with LKB1 deficiency and MCT4 overexpression contributes to the inert TIME. To do this we analyzed the scRNA-seq data from K, KL, and KL MCT4-KO syngeneic tumors. Each type of immune population was well characterized according to the assessment of known cell-type markers and the Immunological Genome Project (ImmGen) dataset.[27]

Among immune subpopulations, the monocyte/macrophage lineage was the most commonly represented (Figure S3A) although the specific monocyte/macrophage phenotypes were markedly impacted by LKB1 and MCT4 depletion. In addition to macrophage, a subset of hypofunctional T cells was also significantly enriched in KL tumors but reversed in KL MCT4-KO tumors (Figure S3A).

Specifically, macrophages in K tumors demonstrated a higher M1 score, while KL tumors were polarized toward higher M2 signature score. These changes induced by LKB1 loss were reversed by MCT4 KO (KL MCT4-KO) which, similar to LKB1-proficient K cells, had a higher M1 signature score[28] (Figures 3A and 3B), supporting a role for MCT4 in mediating the M2 polarization induced by LKB1 loss. Further analysis of macrophages represented by the indicated feature genes identified six different clusters (Figure 3C, Table S1). *Arg1*, a marker of M2 macrophages, was expressed in all clusters except monocyte cluster (c3) (Figure S3B), suggesting that tumor-associated macrophages (TAMs) displayed a general M2 phenotype. To further explore the phenotype of these clusters, we evaluated the M2 and M1 scores in all six clusters (Figure S3D). Among these clusters, cluster 0 (c0) showed a high M2 score, and was marked by high expression of *Vegfa,* enhanced arginine metabolism, and IL8 (Figures S3B and S3C). This population has previously been reported to promote angiogenesis and tumor progression.[29,30] By contrast, c2 expressed *Arg1* and *Il1b* but did not express many other macrophage markers,[31] while c3 and c5 showed high M1 score. Compared with K tumors, KL tumors were particularly highly enriched in c0 and had lower levels of c2. Conversely, KL MCT4-KO tumors reversed the changes observed in KL tumors, with a reduction of c0 compared with KL tumors but increased in c2 (Figure 3D), and an increase in the c3 cluster. Consequently, the M2/M1 ratio was higher in KL tumors compared with K tumors or KL MCT4-KO tumors (Figure 3E). There were no significant changes among the other clusters including *Spp1*$^{+}$ (c4) or *Egr1*$^{+}$ inflammatory (c5) macrophages.

We then evaluated M1 and M2 macrophages by immunofluorescence using murine syngeneic models. Consistent with the scRNA-seq data, KL tumors had significantly higher levels of M2 macrophages ($F4/80^+ARG1^+$ cells), and significantly lower M1 macrophages ($F4/80^+iNOS^+$ cells), compared with K tumors while these changes were reversed by MCT knockout in both LKR13 and LKR10 models (Figures 3F, S3E). To verify that this enhanced M2 polarization was not related to the location of the tumor (e.g. subcutaneous vs. lung), we analyzed tumors from the lungs of GEMMs bearing either *Kras*^{G12D} or *Kras*^{G12D}; *Stk11*$^{fl/fl}$ alleles which confirmed higher levels of M2 macrophages and reduced M1 macrophages in KL tumors (Figure S3F).

KL conditioned medium promotes M2 polarization *in vivo* in an MCT4-dependent manner

We next hypothesized that the M2-polarized phenotype promoted by LKB1 loss was due at least in part to factors secreted by these tumors. To test this, we took implanted gelfoam sponges impregnated with conditioned media from K, KL, or KL MCT4-KO tumor cells subcutaneously in mice,[32] and evaluated macrophage infiltration and polarization after 14 days. The relative abundance of M2 macrophages was significantly higher in gelfoam sponges containing KL-conditioned media than in sponges from K alone, while M1 macrophages showed the opposite trend (Figure 4A). These changes induced by LKB1 loss could be reversed by MCT4 knockout. These data provide evidence that the M2 polarization induced by LKB1 loss was induced at least in part by factors secreted by tumor cells and that these changes were dependent on the lactate transporter MCT4, consistent with a potential role for lactate in promoting M2 polarization.

Suppression of lactate-MCT4 pathway abrogates the M2 polarization induced by LKB1 deficiency

Based on the aforementioned observations, and earlier studies demonstrating that lactate can induce M2 polarization,[33] we hypothesized that the MCT4-dependent shift toward M2 polarization in KL cells may be due to enhanced lactate secretion. To more directly test the impact of the lactate-MCT4 pathway on macrophage polarization *in vitro*, we utilized the established system of Raw264.7 macrophage cell line and freshly isolated peritoneal primary macrophages. As expected, primary macrophages exhibited high expression of macrophage markers including CD11b and CD11c (Figure S4A). These cells were then co-cultured with control media or conditioned medium (CM) from K, KL, and KL MCT4-KO tumor cells. Flow cytometry of $CD206^+$ cells, reflective of an M2 polarized phenotype, demonstrated an increase in M2 polarization when macrophages were cultured with KL-conditioned media, but not K or KL MCT4-KO media. Moreover, the direct addition of lactate in KL MCT4-KO conditioned media significantly increased the percentage of M2 macrophage, while pyruvate or hydrochloric acid which induce a similar pH did not have such significant effects, (Figures 4B and S4B) indicating that the changes were not merely pH-dependent.

We next tested the effects of inhibiting the lactate receptor GPR81 present using 3-Oba (beta-hydroxybutyrate) to antagonize the effects of lactate.[34–36] GPR81 inhibition reversed the M2 polarization induced by KL conditioned media (Figure 4B). Similar results were obtained using primary macrophages (Figure S4B). Moreover, Boyden chamber assay showed enhanced macrophage migration when co-cultured with KL medium compared

to macrophages incubated with conditioned media K or KL MCT4-KO (Figures 4C and S4C); this enhanced migration in KL cells was abrogated by 3-Oba. Phagocytosis has been reported to partially support antigen presentation.[37] We observed that conditioned media from KL tumor cells or media supplemented with lactate decreased phagocytosis (Figures 4D and S4D), while 3-Oba or MCT4-KO CM could reverse this effect. We also investigated additional markers of macrophage polarity and found that RNA levels of M2 markers (*Mcp1* and *Mrc1*) were increased after co-culture with KL-conditioned media, and MCT4 knockdown reversed the effect, while M1 markers showed the opposite trends (Figures 4E and S4E).

Moreover, previous studies indicated that ERK1/2 signaling was associated with M2 macrophages while STAT1 signaling with M1.[38] Concordantly, we also found that conditioned media from KL tumor cells or lactate induced activation of ERK1/2 but not STAT1 in macrophages (Figure S4F). We also observed that PD-L1 expression was increased on Raw264.7 cells treated with KL CM or lactate (Figure S4G). Next, we evaluated the effect of polarized macrophages on T cell killing. Raw264.7 cells were co-cultured with the CM supplemented with either Oba or lactate or sodium lactate for two days. Then, LKR13K-SIINFEKL-expressing cells were used as target cells and cultured with macrophages overnight. OT-I T cells were then added, and cell killing was assessed after 6 h. Treatment with KL CM or lactate promoted the immunosuppressive phenotype of macrophages and inhibited T cell cytotoxicity, and treatment with MCT4-KO CM reversed this effect (Figures 4F, S4H).

LKB1-deficiency is also associated with increased expression of chemokines such as CXCL2 and IL6.[39] To further isolate the effect of lactate, we denatured the CM from K, KL, and KL MCT4-KO tumor cells in effort to inactivate bioactive protein factors. Alternatively, we dialyzed CM to filter low moleculaer weight (MW) (<3 KD) metabolites. Lactate and TGF-β were used as positive controls. Denatured KL CM or exogenous lactate increased CD206 expression on Raw264.7 cells, while filtered medium did not (Figure 4G). Similarly, denatured KL CM retained its ability to increase M2-associated mRNA gene expression and decreased M1-associated genes, but filtered CM did not (Figures 4H, S4I). Taken together, these findings provide further evidence that enhanced lactate secretion associated with LKB1 loss promotes a pro-tumorigenic M2 macrophage polarization that can be reversed by knockout of the lactate transporter MCT4 or lactate receptor blockade.

MCT4 knockout restores CD8$^+$ T cell activity against tumor cells

We next investigated whether T cell hypofunction was also mediated at least in part via the lactate-MCT4 pathway. We incubated the OT-I T cells and LKR13K-SIINFEKL target cells with conditioned media from K, KL, or KL MCT4-KO cells. Compared with conditioned media from K cells, there was significantly less target cell apoptosis induced by T cells in the presence of conditioned media from KL cells (Figure 5A, $p = 0.002$); and this suppression of T cell-mediated apoptosis was largely, but not completely, abrogated when conditioned media from KL cells bearing MCT4-KO was used (Figure 5A, $p = 0.006$, and Figure S5A). We then investigated whether lactate played a role in this suppression of T cell function. The addition of exogenous lactate in KL MCT4-KO medium significantly

suppressed T cell-mediated apoptosis ($p = 0.032$). Moreover, KL CM, or lactate, decreased the percentage of IFN-γ^+ T cell population (Figure 5B), as well as IFN-γ release (Figure S5B). Further analysis indicated that lactate in KL CM, not merely changes in pH, suppressed T cell cytotoxicity function and IFN-γ production (Figures 5C, S5C–S5E). Notably, the suppressive effects of KL CM could also be reversed by 3-Oba (Figures 5C and S5E).

In addition, lactate-enriched medium, as well as KL medium, but not KL MCT4-KO medium, significantly reduced T cell expression of PD-1 and proliferation (Figures S5F–S5G). We further co-cultured T cells with either denatured or filtered CM from K, KL, and KL MCT4-KO, and observed that lactate or the denatured KL CM suppressed T cells function. The filtered KL CM also suppressed T cell-mediated cell-killing, but the effects were less than denatured CM (Figures 5D, S5H). Previous studies also suggested that high lactate in the tumor microenvironment may dampen T cell function by inhibiting glycolysis during T cell activation.[40] Here, we observed similar findings with T cell ECAR decreased in KL CM and reversed by MCT4-KO or 3-Oba (Figure 5E) which suggests that inhibiting the lactate pathway restores T cell metabolism and function. Taken together, these data suggest that the lactate/MCT4 pathways play a role in the suppression of T cell function induced by LKB1 loss.

MCT4 knockout restores cytotoxic CD8$^+$ T cells populations in KL tumors

In addition to the *in vitro* findings, we further observed from the scRNA-seq data that T cells in KL tumor exhibited high exhaustion and STAT3 signaling, while MCT4-KO tumors showed an opposite phenotype and increased PD-1/PD-L1 pathway (Figure 5F). We next took advantage of the T cell inflamed gene expression profile and found MCT4-KO increased some of these genes' expression levels such as *Tigit*, *Cxcl9*, and *Cd274* (Figure S5I).

Importantly, our analysis revealed an increased proportion of hypofunctional T cells in KL tumor compared with K tumors and this increase was reversed by MCT4-KO (Figures 5G, S5J, and Table S2), and this type of T cells showed diminished response to immunotherapy.[41,42] We also investigated the checkpoint/stimulator genes expression in CD8$^+$ T cells from three types of tumors to evaluate their activation status (Figure S5K). The percentage of CD8$^+$ T cells co-expressing stimulators Gitr (*Tnfrsf18*)/4–1bb (*Tnfrsf9*) and checkpoint genes *Pd1*/*Tigit* was high, indicating an activated phenotype in K tumor.[43–46] However, this was dramatically reduced in KL tumors, in which greater than 50% of CD8$^+$ T cells showed lower co-expression. This phenotype was partially reversed by MCT4 knockout in KL MCT4-KO tumors (Figure 5H).

In conclusion, these data indicate that increased lactate in the TIME of LKB1-deficient tumors exerts a negative impact on CD8$^+$ T function, and that focusing a therapeutic strategy on suppressing tumor lactate secretion could enhance cytotoxic T cell activity.

MCT4 loss enhances LKB1-deficient tumors to immune checkpoint blockade therapy

The aforementioned data provides evidence that LKB1 loss results in increased lactate secretion via MCT4, and that this lactate-MCT4 pathway exerts effects on both macrophage

polarization and T cell function. To test the impact of MCT4-KO on tumor growth and whether it could be explained by immune cell effects, we injected LKR13K and LKR13KL cells with or without MCT4 KO in immunodeficient and immunocompetent mice (Figures 6A and 6B). In LKB1-deficient LKR13KL cells, MCT4-KO significantly inhibited tumor growth in immunocompetent, but not immunodeficient, mice (Figure 6A), supporting a role for antitumor immunity in mediating the effects of MCT4-KO. In mice with intact LKB1, however, reduced growth was observed for LKR13K in both immune-competent and immunodeficient models, and MCT4-KO modestly decreased tumor growth in both as well (Figure 6B) suggesting that the impact of MCT4-KO was not dependent on antitumor immunity.

We further explored the effect of MCT4-KO combined with ICB. K tumors with intact LKB1 were responsive to anti-PD1. MCT4-KO significantly reduced tumor growth, and in this model treatment with anti-PD-1 showed no significant inhibition of tumor (Figure 6C). However, in LKB1-deficient tumors that are resistant to PD-1 inhibition,[9,12] we observed that MCT-KO restored responsiveness to anti-PD1 treatment which led to a significant reduction in tumor growth (Figure 6D) and significantly prolonged survival (Figure 6E) compared to mice treated with control antibodies in LKB1-deficient tumors. Similar results were obtained using separate murine tumor models, including LKR10, and 344sq which harbors *Kras*/*Tp53* mutations (Figures 6F–6I). In the LKR10 model, 6 of 18 mice bearing LKR10 KL MCT4-KO tumors treated with anti-PD1 immunotherapy showed a complete tumor regression 60 days post-randomization, whereas none of the 16 mice with KL tumors showed complete regression with anti-PD1 (Figure S6A). Mice bearing LKR10 KL MCT4-KO tumors that had a complete response were re-challenged with a second inoculation four times the amount of the previously injected tumor cell number 4 weeks after tumor regression. All re-inoculated mice showed tumor growth inhibition after 10 days when compared with naive control mice (Figure S6B), suggesting a strong and durable anti-tumor immunity.

To further validate that T cells are critical for inhibiting tumor growth in MCT4-KO tumors treated with anti-PD1, we used anti-CD8 antibody to deplete $CD8^+$ T cells and treated with anti-PD1 on MCT4-KO tumor-bearing mice (Figure S6C). We observed that the depletion of $CD8^+$ T cells completely abrogated the effect of ICB, and tumor growth was accelerated (Figure S6D). Furthermore, MCT4-KO tumors showed a low serum lactate/glucose ratio, suggesting MCT4-KO inhibited lactate export *in vivo* (Figures S6E–S6G), but there was not a significant difference in the intratumoral lactate/glucose level (Figures S6H–S6I).

Collectively, our findings suggested that (i) LKB1 loss led to enhanced lactate secretion via the transporter MCT4; (ii) enhanced lactate in KL medium promoted M2 macrophage polarization and impaired T cell function; (iii) knockout of MCT4 or blocking GPR81 by Oba reversed the immunosuppressive phenotypes; and (iv) KL medium induced immunosuppressive phenotypes could be recapitulated by exogenous lactate or be abrogated by filtering the medium but not by denaturing. These data support the conclusion that blockade of MCT4 and/or disruption of lactate metabolism is a promising therapeutic strategy to increase anti-tumor immune responses of checkpoint inhibition therapy in patients harboring LKB1-deficient LUAD (Figure 6J).

LKB1 loss is associated with reduced T cell infiltration and M2 polarization in LUAD patients

To investigate whether the findings observed in murine models of LKB1-deficient tumors mirror changes observed in patients, we evaluated the relative abundance and localization of immune populations using fluorescent multiplex immunohistochemistry (IHC) from the immunogenomic profiling of NSCLC (ICON) cohort (n = 148, Figure 7A). We observed a low immune cell infiltration associated with LKB1 loss, including reduced $CD3^+$ T, $CD8^+$ T cells, and $CD68^+$ myeloid cells in both tumor and stromal sites (Figures 7B–7D, S7A, and S7B). Then, we utilized array-based expression profiling data from the PROSPECT MDACC dataset (n = 152, 44 cases of LKB1 deficient, 108 cases of LKB1 intact) and performed CIBERSORT[47] to quantify the proportion of macrophages and other immune cells. Consistent with the IHC data, we observed a trend toward a lower proportion of $CD8^+$ T cells in LKB1-deficient tumors compared with LKB1 wild-type (WT) tumors (Figure 7E, $p = 0.073$). Moreover, tumor immune infiltration of M1 macrophages was significantly lower in LKB1-deficient tumors compared to LKB1 WT tumors (Figure S7C). In contrast, there were no significant differences in alternative activated M2 macrophage population between LKB1 WT and LKB1-deficient tumors, which led to a predominantly high M2 ratio in LBK1-deficient tumor samples (median = 0.78, ranges from 0 to 1 vs. median = 0.69, ranges from 0.22 to 1, Figure 7F). Additionally, higher M2 ratio negatively correlated with $CD8^+$ T cells (Figure S7D). CIBERSORT was also performed in TCGA LUAD cohort revealing similar trends, with a marginal increase in M2 ratio and inverse correlation with $CD8^+$ T cells (Figures S7E and S7F). To further validate this finding, we explored the scRNA-seq data of 16 patients with *KRAS* mutant LUAD and identified 11 clusters of myeloid population (Figure 7G). Clusters 1 and 8 corresponded to M2 macrophages as determined by key differentially expressed markers (*CD163*, *MRC1*, *MARCO*, and *TGFB1*). Importantly, we observed that *STK11* mutations were associated with an increased median level of M2 macrophages as a fraction of the total macrophage population (Figure 7H). While the sample size is modest, the observations are consistent with a shift toward M2 polarization in the population of *KRAS* LUAD bearing *STK11* mutations.

Next, we assessed the association between MCT4 expression and M2 macrophages, as well as $CD8^+$ T cells in an LKB1-mutant subgroup from TCGA LUAD. The expression of MCT4 was positively correlated with M2 macrophage level but negatively correlated with $CD8^+$ T cells (Figure 7I). However, we observed no significant correlation in the overall LUAD cohort (Figure S7G). Moreover, in LKB1-mutant patients with high $CD8^+$ T cell infiltration, we observed high MCT4 expression was significantly associated with poor overall survival, but not in patients with low $CD8^+$ T presence (Figure 7J). Altogether, these results indicate that LKB1 loss is associated with lower T cell immune infiltration and function, and with increases in pro-tumoral M2 macrophage polarization, which are associated with MCT4 expression.

DISCUSSION

Immunotherapy with drugs targeting the PD-1-PD-L1 axis has transformed the treatment landscape of NSCLC but the majority of patients experience primary resistance with

objective response rates to ICB monotherapy in the range of ~10–30%.[48–52] Primary resistance to immunotherapy has been associated with low PD-L1 levels and some driver oncogenes such as EGFR and ALK.[53] Recent studies from our group and others have previously demonstrated that alterations in *STK11*/LKB1 in LUAD are associated with an immunosuppressed phenotype[6,9] and primary resistance to ICB, even among patients with high PD-L1 expression or tumor mutational burden (TMB),[9,54] and represent the genomic marker most closely associated with a "cold" immune phenotype.[9] Given its importance as a potential driver of immunotherapy resistance, there remains a major unmet need to better elucidate the mechanisms of this ICB resistance and develop rational therapeutic approaches for overcoming it. Here, we investigate the impact of metabolic alterations induced by LKB1 loss and identify MCT4-dependent lactate secretion as a mediator of this immunosuppression, at least in part via its effects on M2 polarization and effector $CD8^+$ T cell function. This mechanism is not observed in other LUAD subgroups that have similar low response rates to immunotherapy, such as patients bearing EGFR mutation.[53,55] Our study, therefore, highlights the lactate-MCT4 axis is a relevant therapeutic target for these patients with limited therapeutic alternatives.

The LKB1 protein is known to serve as a master regulator of cellular metabolism and growth, exerting its effects via regulation of downstream kinases including AMPK and SIKs.[15,17,18] Tumors lacking LKB1 expression undergo metabolic reprogramming characterized by an increased glycolytic rate and glutaminolysis dependence.[20,56] Several studies have reported that dysregulation of the LKB1-AMPK axis promotes a metabolic switch to aerobic glycolysis which is associated with enhanced lactate production and secretion in LKB1-deficient tumors.[19,57,58] Consistent with earlier studies, we find that LKB1 loss leads to a marked upregulation in lactate secretion as well as a metabolic shift toward higher glycolysis, lower oxygen consumption, and a reduced OXPHOS phenotype. Notably, using isogenic human and murine cells as well as genetically engineered mouse (GEM) models, we also find that LKB1 loss is associated with upregulation of MCT4, one of two major transporters (along with MCT1) known to promote lactate secretion, glycolysis, tumor cell invasion, metastases, and tumor growth,[59–65] and to be associated with poor outcome in NSCLC and other solid tumors.[24] Highlighting its importance in these metabolic changes, we find that depletion of MCT4 essentially abrogates the increase in extracellular lactate induced by LKB1 loss and increases intracellular lactate with a concomitant decrease in intracellular pH. Interestingly, while MCT1 has been found to be upregulated in some cancers,[66–68] we observed upregulation of MCT4, but not MCT1, following LKB1 loss.[69] Recent studies indicated that MCT4 expression was associated with mitochondrial NADH dehydrogenase (*ND*) mutation.[25] We observed that in H358 cells which harbors mutant *ND*, MCT4 is highly expressed and knockdown of LKB1 does not cause a further increase in MCT4 expression, suggesting that the impact of LKB1 on MCT4 may be most pronounced in cells with WT *ND*, and that *ND* mutation may be a dominant regulator of MCT4 expression.

Given the known immunosuppressive effects of lactate,[70–74] we next investigated whether the MCT4/lactate pathway played a role in the ICB resistance and immunosuppressed phenotype observed in LKB1-deficient tumors. Previous studies have suggested that lactate-induced M2 macrophage polarization,[33,75,76] modulated MDSCs and T cell function, and

that inhibition of the lactate receptor GPR81 promoted a pro-inflammatory macrophage response.[77] First, we investigated the tumor microenvironment of immune-competent KRAS mutant murine models using scRNA-seq and found that LKB1 loss led to a striking shift in the macrophage phenotype toward M2 polarization, an observation supported by our analysis of clinical specimens from LUAD patients harboring WT or *STK11*/LKB1-mutation. These data highlight a previously unappreciated aspect of the immune phenotype of these tumors, which have been reported to have lower levels of T cell infiltration, PD-L1, IFN-γ signaling,[6,12] stimulator of interferon genes (STING) expression,[78] and higher levels of granulocytic myeloid-derived suppressor cells (G-MDSCs)[79] and immunosuppressive cytokines such as IL-6 [12]. Based on single-cell RNA-seq and functional studies using SIINFEKL peptide-expressing tumor cells, we also observed not only lower levels of $CD8^+$ T cells but also evidence of hypofunctional $CD8^+$ T cells or a late stage of T cell exhaustion, changes which were also reversed by MCT4 knockout. This phenotype of hypofunctional or exhausted T cells has been associated with reduced ICB benefit.[45] These data, taken together with other recent studies,[12,79] support the model that LKB1-mediated immunosuppression involves multiple immune subpopulations, including increased M2 polarization and suppression in the number and function of effector $CD8^+$ T cells.

We then investigated whether these changes were dependent on the lactate/MCT4 axis. MCT4 knockout could reverse the M2 polarization observed *in vivo* using murine models, as well as *in vitro* using conditioned media from LKB1-deficient cells. Similar changes were also observed using a modulator of the lactate receptor GPR81. Although GPR81 inhibitors are currently unavailable,[80] several studies have shown the equivalent effects of 3-Oba treatment compared to GPR81 knockdown,[81–83] suggesting using 3-Oba to suppress lactate-mediated GPR81 activation. MCT4 knockout and GPR81 inhibition also reversed some, but not all, of the effects on T cell subpopulations induced by LKB1 loss such as a reduction in the hypofunctional T cell population. More importantly, in three different LKB1-deficient murine LUAD models that were completely resistant to PD-1 inhibition, MCT4 knockout restored responsiveness to PD-1 inhibition to levels similar to that of LKB1-intact tumors,[9] supporting the biological significance of the lactate/MCT4 axis.

These findings have significant mechanistic and therapeutic implications. Our data further elucidate the immunosuppressive phenotype of LKB1-deficient LUAD tumors, including increased M2 polarization and hypofunctional or exhausted $CD8^+$ T cells. Our study also demonstrates, for the first time, that enhanced MCT4-dependent lactate secretion is a mediator of at least some of these changes, and that targeting this pathway at the level of the MCT4 transporter or lactate receptor can abrogate M2 polarization, restore certain aspects of T cell function, and overcome the PD-1 inhibitor resistance induced by LKB1 loss. It is noteworthy, therefore, that MCT4 inhibitors or dual MCT1/4 inhibitors have shown promising anti-tumor effects in pre-clinical models.[84] One limitation of the current report is that the findings are largely based on animal models. Additional work will be required to establish the clinical relevance in human KRAS-LKB1 mutant NSCLC. Our data do not rule out that other potential mechanisms such as suppressed STING expression[78] or increased G-MDSCs[79] or cytokine expression may contribute to the observed ICB resistance. Our findings do, however, provide evidence that targeting the MCT4-lactate axis may enhance

antitumor immunity and ICB response in LKB1-deficient LUAD and that this approach merits further investigation for this recalcitrant population.

STAR★METHODS

RESOURCE AVAILABILITY

Lead contact—Further information and requests for resources and reagents should be directed to and will be fulfilled by the Lead Contact, John V. Heymach (jheymach@mdanderson.org).

Materials availability—This study did not generate new unique reagents.

Data and code availability—Datasets are publicly available in the Gene Expression Omnibus (GEO) database under accession codes (GEO: GSE231742). All computer code used in this study is publicly available, as listed in the key resources table. All data are available upon request.

EXPERIMENTAL MODEL AND STUDY PARTICIPANT DETAILS

Human tumor specimens—A total of 16 LUAD samples from Massachusetts General Hospital were analyzed in this study. 11 samples with *KRAS* mutation/*STK11* wild-type, and 5 samples with *KRAS*/*STK11* co-mutation. Institutional Review Boards at MGH approved protocols for tissue collection used for sequencing. Informed consent was obtained from all subjects prior to collection.

Cell lines and culture—Human *Kras*/*Stk11* mutant cell lines A549, H460 and H2030 and their paired LKB1 overexpression cells were used. H358, H441, H2009, H1792, H2122, HCC44, H1355, H1944 were used. Murine cell lines LKR10 and LKR13 and isogenic pair K, KL, and 344sq cells were. Cells were maintained in RPMI1640 medium supplemented with glutamine, 10% fetal bovine serum and 1% penicillin-streptomycin. HEK293T, Phoenix cells and Raw264.7 cells were maintained in DMEM medium. All the cell lines were authenticated by short tandem repeat analysis and mycoplasma test.

For establishing LKB1 kinase dead protein overexpressing cells, 2μg pBABE-FLAG-KD LKB1 plasmid was transfected into Phoenix cells using lipofectamine 2000. After 48h, supernatant was collected and filtered by 0.45μM filter, then added into A549 and H460 cells with polybrene (2μg/ml) for 2days, and the stable cell lines were selected by puromycin.

Mouse model—The mice were maintained in The Research Animal Support Facility, and all animal experiments were conducted according to the protocols approved by the Institutional Animal Care and Use Committee (Approved number: 00001213-RN03). For Genetically engineered mouse (GEM) model, *Kras*^{G12D} (K) mice and *Kras*^{G12D}; *Stk*11$^{fl/fl}$ (KL) mice were used. Briefly, K mice (4 female and 3 male) and KL mice (3 female, 3 male) were treated with Adenovirus-Cre through inhalation at the age of 6 weeks. Six to nine weeks after Adenovirus-Cre administration, the mice were sacrificed, and the lung tumor nodules were harvested for the further analysis. C57BL/6 Tg(TcraTcrb)1100Mjb (OT-

I mice) were purchased from Jackson Laboratory. Mice were maintained in pathogen-free conditions and the spontaneous lung tumors were collected at designated time points.

METHOD DETAILS

Opal multiplexed IHC staining and imaging—The formalin-fixed paraffin-embedded tissue microarray containing human LUAD was acquired from MD Anderson Cancer Center. The slides were processed using the Opal 7 manual kit. Images were captured and analyzed by pathologists at Department of Translational Molecular Pathology.

***In vivo* studies—**For nude mice experiment, LKR13K and LKR13KL cells ($1.8*10^6$) with or without MCT4-KO were injected into the right flank of the mice at the ages of about 8 weeks. Tumor growth was measured three times a week.

For the syngeneic mouse model, LKR10KL, LKR13KL, 344sqKL with or without MCT4 knock out (KO) murine LUAC cells ($1*10^6$) were injected subcutaneously into the right flank of syngeneic recipient male mice (129SV genetic background) at the ages of 6–8 weeks. Mice bearing tumors around 150–250mm^3 were randomly assigned to i.p. treated with 200mcg anti-PD-1 (clone RMPI-14, BioXCell) or isotype control IgG (clone 2A3, BioXCell) twice a week. Tumor growth was measured three times a week, and when the tumor volume reached 2000mm^3, the mice were sacrificed. For 344sqKL model, we set the endpoint as the tumor volume reached 1000 mm3. Tumor tissues were frozen in liquid nitrogen, embedded with OCT or formalin fixed, paraffin embedded for histological analysis. To deplete $CD8^+$ T cells, 200mcg anti-CD8 antibody was i.p. injected into the mice on day −1, 2, 6, 9, 13, 16, total six doses.

Establishing knock out cell lines by CRISPR/Cas9—Knock out of MCT4 was performed by transfecting MCT4 CRISPR-Cas9 plasmid (Santa Cruz Biotechnology, USA, sc-429828). Expressing gRNA sequences are derived from the GeCKO (v2) library and the Cas9 protein to induce a site-specific double strand break (DSB) in the genomic DNA. Cells were plated into 12-wells plate and transfection was performed using Lipofectamine 2000 (Life Technologies, Carlsbad, CA, USA) according to the manufacturer's instruction. After 48h, GFP^+ cells were sorted into 96-wells plates for single clone selection. MCT4 lack of expression was confirmed by western blotting. For knockout human or mouse LKB1, LKB1 CRISPR/Cas9 KO plasmid (h) or LKB1 CRISPR/Cas9 KO plasmid (m) were transfected into human cell lines and 344sq cells, respectively. Single LKB1 KO 344sq cell was sorted by flow cytometry and the LKB1 KO was confirmed by western blot.

Western blotting—Western blot was performed as described previously.[7] The total protein concentration was calculated using BCA Assay kit. The primary antibodies were incubated overnight at 4°C. The membranes were developed using ECL method.

Reverse-phase protein arrays (RPPAs)—Protein was extracted from tumor tissues, and RPPAs were performed as previously described.[92] MCT4 primary antibody was purchased from Milllipore (AB3314P). RPPA data were analyzed using SuperCurve method, and the protein levels were detected by MicroVigene software and R package developed at MDACC.

Quantative real-time PCR (qRT-PCR)—Total RNA was isolated using the RNeasy Plus Mini Kit (74136, Qiagen). First strand cDNA was synthesized by SuperScript™ III First-Strand Synthesis System (18080051, ThermoFisher) according to the manufactures' protocol. qRT-PCR was performed with PerfeCT SYBR Green Fast Mix (95074–012, Quantabio) and various primers at ABI7500 FAST real-time PCR system (ThermoFisher). Actin was used as internal control.

Cell viability—$1*10^3$ indicated Cells were plated into 6-well plates and cultured in normal condition for colony formation for 10–14 days. Then cells were fixed and stained with 0.5% crystal violet and analyzed by Image J. The assays were repeated at least times independently.

Flow cytometry—Cells were harvested into single cell suspension. For cell surface markers such as CD206, PD-L1, PD1, cells were stained with fluorescently conjugated antibodies or dye according to the manufacturer's instructions. For intracellular TNF and IFN-γ staining, cells were fixed, permeabilized and stained according to the manufacture's protocol. Flow cytometric analysis was performed on a BD FACSCanto II system and data were analyzed with FlowJo v10 software.

Lactate/glucose detection—Cells were plated into 6-wells plate at a density of 2×10^5 cells/well for culturing 24h. Both cell lysis and medium were collected. For cell lysis, resuspend cell in 100ul assay buffer and sonicated for 3min (10s on, 12s off, 240W). Then centrifuge and collect the supernatant. lactate detection was performed using Assay kits (ScienCell, Carlsbad, CA, USA, #8308) following the manufacturer's instruction then normalized to total protein.

To measure serum and intratumoral lactate and glucose, we sacrificed the mice, and collected the serum and tumor samples. Serum samples were diluted with PBS only; for tumor samples, flash frozen tumors were minced into powder in liquid nitrogen and resuspended in PBS. Lactate level and glucose level were detected with Lactate-Glo™ Assay kit (J5022) and Glucose-Glo™ Assay (J6021, Promega) according to the manufactures' instruction.

Metabolic assays—Cell oxygen consumption rate (OCR) and extracellular acidification rate (ECAR) were measured using Seahorse XF96 system according to the protocol. Briefly, tumor cells or macrophages at density of $1.5*10^4$/well were seeded into XF96 plates overnight and then changed into XF medium. Cell bioenergetics were assessed through subsequently adding glucose (10mM), oligomycin (1.5μM), and 2-deoxyglucose (2-DG, 50mM); or oligomycin (1.5μM), carbonyl cyanide-4 (trifluoromethoxy) phenylhydrazone (FCCP, 0.5μM) and rotenone/antimycin (Rot/AA, 0.5μM). Data were normalized to cell number and processed by Wave software (Agilent). Bioenergetic capacity was calculated based on the protocols developed by Mookerjee et al. and the basal level was measured at culture conditions.

Intracellular pH assay—To assess cytosolic pH, cells were plated into 12-wells plate and stained with pHrodo™ Red AM dye in HBSS-free buffer, and DAPI for 20min. Then, cells

were pictured under fluorescence microscopes and the fluorescence was measured by BD FACSCanto II system.

Single-cell RNA sequencing (scRNA-seq)—1×10^6 LKR13 K, LKR13 KL and LKR13 KL MCT4KO cells were injected into the flack of 129SV mice. When tumor volume reached 500 mm^3-700mm^3, tumors were harvested and dissociated in single cells suspension according to the protocol. Briefly, tumor tissues were mechanically disrupted and digested with Collagenase A, hyaluronidase, Dispase and DNase I. Then suspended cells were passed through a 40μm strainer and treated with ammonium chloride to remove red blood cells for further processing. Single cell cDNA library was prepared and sequenced at the University of Texas MD Anderson Cancer Center Sequencing Core using the 10X Genomics platform.

Immunofluorescence staining—Frozen sections were fixed in cold acetone, acetone/chloroform (1:1, v/v) and acetone for each 5 min, then washed with PBS. The slides were blocked using PBS containing 5% horse serum and 1% goat serum for 20min and incubated with primary antibody overnight at 4°C. The next day, sections were washed 3 times with PBS and incubated with block solution for 10min and then secondary antibody for 1h. Sections were washed with PBS and stained with DAPI mount for imaging. The primary antibodies were anti-iNOS (Thermo, 1:200), anti-F4/80 (abcam, 1:200), anti-ARG1 (Cell signaling Technology, 1:50), anti-MCT4 (Santa Cruz, 1:50). The secondary antibodies were Alexa Fluor488 anti-Rabbit IgG (1:400), Alexa Fluor488 anti-mouse IgG (1:400), Alexa Fluor594 anti-Rat IgG (1:400).

For evaluating the staining score, Fiji/Image J with coloc 2 was used and the percentage of double positive cells were measured.

***In vivo* macrophage attraction assay—**Sterile gelfoam sponges were cut into 5 mm^3 sections and hydrated in PBS overnight. PBS was removed and a solution of 0.4% agarose containing either PBS or conditioned medium from K, KL, and KL MCT4-KO cell lines was added to each sponge. The sponges were incubated at room temperature for 1h and implanted subcutaneously into mice. Two weeks later, sponges were harvested, embedded with OCT and cut as frozen sections.

***Ex vivo* macrophage polarization—**Peritoneal macrophages were isolated as previously described.[93] Briefly, 2ml of 4% Brewer thioglycollate medium was injected into the peritoneal cavity of C57BL/6 mice. After 4 days, the mice were anesthesia and euthanized. Inject 10ml cold PBS through peritoneal wall and aspirate fluid from peritoneum. Centrifuge and resuspend cell pellet in cold DMEM medium.

To induce the M2 polarization, the primary peritoneal macrophages were treated with conditioned medium (CM) for 2 days. Additional treatment included lactate (10mM), sodium lactate (10mM), sodium pyruvate (10mM), sodium 3-hydroxybutyrate (8mM), hydrogen chloride. The mRNAs of target genes were measured and the percentage of M2 was tested using flow cytometry by labeling with anti-mouse CD206 antibody. The mobility of polarized macrophages was performed using the transwell (BD). Primary macrophages

were seeded at a density of $2*10^5$ cells/well to top chamber with 8μM pore, and co-cultured with CM in the bottom for 24hours. Migrated cells were stained using crystal violet.

For the phagocytosis analysis, Raw264.7 or peritoneal macrophages were cultured with the specified conditioned medium for two days. LKR13K cells were labeled with MitoTracker™ Deep Red for 30 minutes, trypsinized, and co-cultured with the macrophages for 10 minutes. After washing the cells, the fluorescent fractions within the macrophages were quantified by flow cytometry.

T cell stimulation assay was performed by co-culturing polarized macrophages, OT-I $CD8^+$ T cells and SIINFEKL target cells together. Briefly, Raw264.7 cells were co-cultured with the specified conditioned medium supplemented with either Oba or lactate or sodium lactate for 2 days. Then, LKR13K-SIINFEKL expressing cells were added and co-cultured overnight. The following day, OT-I T cells were added and cell killing and IFN-γ expression were measured after 6 hours.

To determine the effect of lactate, the conditioned mediums from K, KL and KL MCT4-KO were boiled for 5min or dialyzed by centrifuging using 3000 Dalton MW cutoff filters at 4000g for 30min. Then, these mediums were used for the following experiments.

T cell functional assay—$CD8^+$ T cells were isolated from spleens of OT-1 mice using EasySep™ Mouse $CD8^+$ T Cell Isolation Kit (Stemcell Technologies). $CD8^+$ T were stimulated by anti-CD3 (0.5μg/ml) and anti-CD28 (5μg/ml) pre-coated plates for 2days and maintained in RPMI1640 medium with 2-mercaptoethanol (50μM), 1% ITS. Then T cells were expanded with IL2 (0.4ng/ml). All reagents were from Gibco.

SIINFEKL peptide was overexpressed in murine *Kras* LKR13 (LKR13K-SIINFEKL) tumor cells to serve as a target for OT-I cells. *In vitro* T cell killing assay were performed by co-culturing the SIINFEKL expressing target cells with $CD8^+$ T treated with different conditioned medium, with or without the addition of lactate (10mM), sodium lactate (10mM), sodium pyruvate (10mM), sodium 3-hydroxybutyrate (8mM), or hydrogen chloride. Target cells were labeled with Mitotracker Deep Red (M22426, Thermo, 100nM) for 30min at 37°C. Then, adding T cells and Incucyte® Caspase-3/7 Green Reagent (4440, Essen Bioscience). Cell viability was monitoring and analyzed using Incucyte Live-Cell Assays (Sartorius).

To establish luciferase reporter cells, pHIV-luc-zsgreen, pMD2.G and psPAX2 plasmids were co-tranfected to 293T cells. Lentivirus was collected after 72hours and filtered using 0.45μM filter. LKR13K expressing SIINFEKL cells were infected with pHIV-luc-zsgreen lentivirus, and GFP positive cells were selected. To detect the T cell killing by luciferase reporter, after co-culturing target cells with T cells, removed medium and added 150μg/ml D-luciferin and incubated for 10min. The luciferase activity was measured by FLUOstar OPTIMA microplate reader. The T cell killing was calculated as follows: cell lysis%=(Value $_{neg}$ -Value $_{detect}$)/Value $_{neg}$×100.

IFN-γ expression was detected using ELISA MAX™ Standard Set Mouse IFN-γ (430801, BioLegend) according to the protocol. To measure the intracellular TNF/IFN-γ, T cells with

different CM treatment were co-cultured with SIINFEKL target cells for 6hours, and then T cells were collected and fixed. After permeabilization, T cells were stained with PerCP-TNF and PE-IFN-γ, and then analyzed by flow cytometry. To measure cells proliferation, after IL2 expansion for 1day, T cells were labeled by CFSE (C34554, Thermo, 5μM in PBS) and cultured in medium with conditioned medium for 4–5 days and then detected by flow cytometry.

To measure the metabolism of T cells, 2×10^5 cells/well were added into Seahorse cell culture plate and centrifuged at 400g for 5mins, and then detected according to the protocol.

QUANTIFICATION AND STATISTICAL ANALYSIS

Unsupervised clustering analysis—The raw scRNA-seq data were preprocessed using the Cell Ranger pipeline analysis provided by 10×Genomics. After data filtering, doublets removal, batch-effect evaluation and data normalization as described previously,[94] "Seurat" R package (v3.1.5) was used to analyze the normalized gene-cell matrix. Each cluster was determined by highly variable genes identified with *FindClusters* function. For visualization, the dimensionality was further reduced using t-SNE or UMAP methods with *RunTSNE* and *RunUMAP* functions.

Deferentially expressed genes (DEGs) and pathway enrichment analysis—We identified DEGs with *FindMarkers* function. The DEGs list was filtered with expression fold change, q value and then as input for Ingenuity Pathway Analysis (Qiagen). Pathway enrichment was visualized with "ggplot2" package. Gene set variation analysis by "GSVA" package (v1.36.2) was used for gene set enrichment analysis. For the gene signature score, we used *AddModuleScore* function. The phagocytosis related genes include *Msr1*, *Mertk*, *C1qb*, *Cd36*, *Cd47*, *Clec9a*, *Adgrb1*, *Itgam*, *Clec12a*, *Fcgr2* and *Mrc1*; the angiogenesis related genes include *Vegfa*, *Nrcam*, *Vcan*, *Pdgfb*, *Fhl3*, *Ang2*, *Mmp12*, *Serpine1* and *Tgfb1*; the glycolysis related genes include *Eno1*, *Gapdh*, *Pkm*, *Slc16a3*, *Eno2*, *Hk1*, *Pgam1*, *Ldha*, *Pfkl*, *Pfkp*, *Tpi1*,*Slc2a1*, *Hk2*, *Eno3*, *Slc16a1*, *Aldoa*, *Pgam2*, *Pfkm*, *Pklr* and *Ldhb*; the OXPHOS related genes include *Acly*, *Aco1*, *Aco2*, *Cs*, *Dlat*, *Dld*, *Dlst*, *Idh1*, *Idh2*, *Idh3a*, *Idh3b*, *Mdh1*, *Ogdh*, *Ogdhl*, *Pck1*, *Pck2*, *Pdha1*, *Pdhb*, *Sdhc*, *Sucla2*, *Suclg1* and *Suclg2*; M1 related genes include *Ccl3*, *Ccl4*, *Prf1*, *Il6*, *Irf5*, *Cxcl10*, *Il1b*, *Ccl12*, *Tnf*, *Cd86*, *Ifng*, *Tbx21*, *Il17a*, *Cd8a*, *Il2*, *Il12a*; M2 related genes include *Arg1*, *Cd74*, *Ptgs2*, *Vegfa*, *Ciita*, *Il10*, *Mmp12*, *Mif*, *Cd274*, *Mrc1*, *Msr1*, *Csf1r*, *Il1r2*, *Csf2*, *Ctla4*.

SPICE (simplified presentation of incredibly complex evaluations) charts analysis—The expression of indicated markers in $CD8^+$ T cells were evaluated in each types of tumors. Excel sheet containing all the cells and relative frequencies of cells in each combination of co-expression was created, converted to a spice-compatible file and pie charts were visualized with SPICE (v6).

Trajectory analysis—"Monocle 2" package was applied to the trajectory analysis. Dimensionality reduction was done using *DDRTree* method, and cells were ordered by *orderCells* function.

Analysis of immune cell infiltration, MCT4 expression and outcomes in TCGA dataset—Infiltration estimation, MCT4 expression and survival data for all LUAD were extracted from TIMER2.0 and TCGA dataset, respectively. Kaplan-Meier curve was generated by splitting the patients with expression percentage (50%) and infiltration percentage (50%).

Statistical analysis—Mann-Whitney test was used to measure the difference between each group in clinical samples. Survival was analyzed using Logrank test. Two-sided student's t test and 2-way ANOVA were used to detect the statistical significance between each group from preclinical experiments. Statistical analysis was performed in GraphPad Prism 8 software. P value less than 0.05 was considered statistically significant. *, $p<0.05$, **, $p<0.01$, ***, $p<0.001$.

Supplementary Material

Refer to Web version on PubMed Central for supplementary material.

ACKNOWLEDGMENTS

We thank Dr. Monique Nilsson for the constructive discussions and editorial assistance. The study was supported by The Lung SPORE P50CA070907-01, CPRIT RP160652, P30 CA016672, The Stand Up To Cancer Foundation, Mark Foundation, Cain Foundation, the Rexanna Foundation, Carrico and Isaacson Memorial Fund, Tonti Fund, Gunnigar Fund, Mugnaini Fund, and the Ford Petrin Fund.

F.S. has held stock ownership in BioNTech SE and Moderna Inc; has received honoraria from Bristol Myers Squibb and RV Mais Promocao Eventos LTDS; has received institutional research funding from Amgen, Mirati Therapeutics, Boehringer Ingelheim, Merck & Co, Novartis, and Pfizer; has an immediate family member who has received research funding from AImmune Therapeutics; and has been reimbursed for travel, accommodations, or other expenses by Tango Therapeutics, Amgen, and AstraZeneca Pharmaceuticals. T.M. is a consultant for Immunos Therapeutics, Daiichi Sankyo Co and Pfizer; is a cofounder of and equity holder in IMVAQ Therapeutics; receives research funding from Bristol-Myers Squibb, Surface Oncology, Kyn Therapeutics, Infinity Pharmaceuticals, Peregrine Pharmaceuticals, Adaptive Biotechnologies, Leap Therapeutics, and Aprea Therapeutics; is an inventor on patent applications related to work on oncolytic viral therapy, alpha virus-based vaccine, *neo* antigen modeling, CD40, GITR, OX40, PD-1, and CTLA-4. J.D.W. is a consultant for Apricity, Ascentage Pharma, Arsenal IO, Astellas, AstraZeneca, Bicara Therapeutics, Boehringer Ingelheim, Bristol Myers Squibb, Chugai, Daiichi Sankyo, Dragonfly, Georgiamune, Idera, Imvaq, Kyowa Hakko Kirin, Maverick Therapeutics, Psioxus, Recepta, Tizona, Trieza, Trishula, Sellas, Surface Oncology, Werewolf Therapeutics; receives Grant/Research Support from Bristol Myers Squibb, Sephora; has Equity in Tizona Pharmaceuticals, Imvaq, Beigene, Linneaus, Apricity, Arsenal IO, Georgiamune, Trieza, Maverick, Ascentage. K.K.W. is a founder and equity holder of G1 Therapeutics; has sponsored Research Agreements with MedImmune, Takeda, TargImmune, Mirati, Merus, Alkermes and BMS; has consulting & sponsored research agreements with AstraZeneca, Janssen, Pfizer, Novartis, Merck, Ono, Array. R. J. D. is a member of the Scientific Advisory Board for Agios Pharmaceuticals and Vida Ventures. J.D.M receives licensing fees from the NCI and UT Southwestern to distribute cell lines. N.I.V. receives consulting fees from Sanofi, Regeneron, Oncocyte, and Eli Lilly, and research funding from Mirati. J.F.G. has served as a compensated consultant or received honoraria from Bristol-Myers Squibb, Genentech/Roche, Takeda, Loxo/Lilly, Blueprint Medicine, Gilead, Moderna, AstraZeneca, Curie Therapeutics, Mirati, Merus Pharmacueticals, Nuvalent, Pfizer, Novartis, Merck, iTeos, Karyopharm, and Silverback Therapeutics; research support from Novartis, Genentech/Roche, and Takeda; institutional research support from Bristol-Myers Squibb, Tesaro, Moderna, Blueprint, Jounce, Array Biopharma, Merck, Adaptimmune, Novartis, and Alexo; equity in AI Proteins, and has an immediate family member who is an employee with equity at Ironwood Pharmaceuticals. A.R. receives honoraria from Adaptive Biotechnologies; is a member of advisory board for Adaptive Biotechnologies. J.V.H. is a member of advisory committees of AstraZeneca, EMD Serono, Boehringer-Ingelheim, Catalyst, Genentech, GlaxoSmithKline, Guardant Health, Foundation medicine, Hengrui Therapeutics, Eli Lilly, Novartis, Spectrum, Sanofi, Takeda, Mirati Therapeutics, BMS, BrightPath Biotherapeutics, Janssen Global Services, Nexus Health Systems, Pneuma Respiratory, Kairos Venture Investments, Roche, Leads Biolabs, RefleXion, Chugai Pharmaceuticals; has research support from AstraZeneca, GlaxoSmithKline, Spectrum; has royalties and licensing fees from Spectrum.

REFERENCES

1. Cancer Genome Atlas Research Network (2014). Comprehensive molecular profiling of lung adenocarcinoma. Nature 511, 543–550. 10.1038/nature13385. [PubMed: 25079552]
2. Ji H, Ramsey MR, Hayes DN, Fan C, McNamara K, Kozlowski P, Torrice C, Wu MC, Shimamura T, Perera SA, et al. (2007). LKB1 modulates lung cancer differentiation and metastasis. Nature 448, 807–810. 10.1038/nature06030. [PubMed: 17676035]
3. Gillette MA, Satpathy S, Cao S, Dhanasekaran SM, Vasaikar SV, Krug K, Petralia F, Li Y, Liang WW, Reva B, et al. (2020). Proteogenomic characterization reveals therapeutic vulnerabilities in lung adenocarcinoma. Cell 182, 200–225.e35. 10.1016/j.cell.2020.06.013. [PubMed: 32649874]
4. Gill RK, Yang SH, Meerzaman D, Mechanic LE, Bowman ED, Jeon HS, Roy Chowdhuri S, Shakoori A, Dracheva T, Hong KM, et al. (2011). Frequent homozygous deletion of the LKB1/STK11 gene in non-small cell lung cancer. Oncogene 30, 3784–3791. 10.1038/onc.2011.98. [PubMed: 21532627]
5. Calles A, Sholl LM, Rodig SJ, Pelton AK, Hornick JL, Butaney M, Lydon C, Dahlberg SE, Oxnard GR, Jackman DM, and Jänne PA (2015). Immunohistochemical loss of LKB1 is a biomarker for more aggressive biology in KRAS-mutant lung adenocarcinoma. Clin. Cancer Res. 21, 2851–2860. 10.1158/1078-0432.CCR-14-3112. [PubMed: 25737507]
6. Skoulidis F, Byers LA, Diao L, Papadimitrakopoulou VA, Tong P, Izzo J, Behrens C, Kadara H, Parra ER, Canales JR, et al. (2015). Co-occurring genomic alterations define major subsets of KRAS-mutant lung adenocarcinoma with distinct biology, immune profiles, and therapeutic vulnerabilities. Cancer Discov. 5, 860–877. 10.1158/2159-8290.CD-14-1236. [PubMed: 26069186]
7. Sitthideatphaiboon P, Galan-Cobo A, Negrao MV, Qu X, Poteete A, Zhang F, Liu DD, Lewis WE, Kemp HN, Lewis J, et al. (2021). STK11/LKB1 mutations in NSCLC are associated with KEAP1/NRF2-dependent radiotherapy resistance targetable by glutaminase inhibition. Clin. Cancer Res. 27, 1720–1733. 10.1158/1078-0432.CCR-20-2859. [PubMed: 33323404]
8. Arbour KC, Jordan E, Kim HR, Dienstag J, Yu HA, Sanchez-Vega F, Lito P, Berger M, Solit DB, Hellmann M, et al. (2018). Effects of Co-occurring genomic alterations on outcomes in patients with KRAS-mutant non-small cell lung cancer. Clin. Cancer Res. 24, 334–340. 10.1158/1078-0432.CCR-17-1841. [PubMed: 29089357]
9. Skoulidis F, Goldberg ME, Greenawalt DM, Hellmann MD, Awad MM, Gainor JF, Schrock AB, Hartmaier RJ, Trabucco SE, Gay L, et al. (2018). STK11/LKB1 mutations and PD-1 inhibitor resistance in KRAS-mutant lung adenocarcinoma. Cancer Discov. 8, 822–835. 10.1158/2159-8290.CD-18-0099. [PubMed: 29773717]
10. Facchinetti F, Bluthgen MV, Tergemina-Clain G, Faivre L, Pignon JP, Planchard D, Remon J, Soria JC, Lacroix L, and Besse B (2017). LKB1/STK11 mutations in non-small cell lung cancer patients: descriptive analysis and prognostic value. Lung Cancer 112, 62–68. 10.1016/j.lungcan.2017.08.002. [PubMed: 29191602]
11. Li H, Liu Z, Liu L, Zhang H, Han C, Girard L, Park H, Zhang A, Dong C, Ye J, et al. (2022). AXL targeting restores PD-1 blockade sensitivity of STK11/LKB1 mutant NSCLC through expansion of TCF1(+) CD8 T cells. Cell Rep. Med. 3, 100554. 10.1016/j.xcrm.2022.100554.
12. Koyama S, Akbay EA, Li YY, Aref AR, Skoulidis F, Herter-Sprie GS, Buczkowski KA, Liu Y, Awad MM, Denning WL, et al. (2016). STK11/LKB1 deficiency promotes neutrophil recruitment and proinflammatory cytokine production to suppress T-cell activity in the lung tumor microenvironment. Cancer Res. 76, 999–1008. 10.1158/0008-5472.CAN-15-1439. [PubMed: 26833127]
13. Carretero J, Shimamura T, Rikova K, Jackson AL, Wilkerson MD, Borgman CL, Buttarazzi MS, Sanofsky BA, McNamara KL, Brandstetter KA, et al. (2010). Integrative genomic and proteomic analyses identify targets for Lkb1-deficient metastatic lung tumors. Cancer Cell 17, 547–559. 10.1016/j.ccr.2010.04.026. [PubMed: 20541700]
14. Li R, Salehi-Rad R, Momcilovic M, Lim R, Ong S, Huang Z, Tran L, Zhe J, Paul M, Teitell M, et al. (2020). A11 blockade of myeloid suppressor cells overcomes the anti-PD-1/PD-L1 resistance in KRAS-driven and LKB1-deficient NSCLC. J. Thorac. Oncol. 15, S15. 10.1016/j.jtho.2019.12.040.
15. Shackelford DB, and Shaw RJ (2009). The LKB1-AMPK pathway: metabolism and growth control in tumour suppression. Nat. Rev. Cancer 9, 563–575. 10.1038/nrc2676. [PubMed: 19629071]

16. Faubert B, Solmonson A, and DeBerardinis RJ (2020). Metabolic reprogramming and cancer progression. Science 368, eaaw5473. 10.1126/science.aaw5473.
17. Hollstein PE, Eichner LJ, Brun SN, Kamireddy A, Svensson RU, Vera LI, Ross DS, Rymoff TJ, Hutchins A, Galvez HM, et al. (2019). The AMPK-related kinases SIK1 and SIK3 mediate key tumor-suppressive effects of LKB1 in NSCLC. Cancer Discov. 9, 1606–1627. 10.1158/2159-8290.CD-18-1261. [PubMed: 31350328]
18. Murray CW, Brady JJ, Tsai MK, Li C, Winters IP, Tang R, Andrejka L, Ma RK, Kunder CA, Chu P, and Winslow MM (2019). An LKB1-SIK Axis suppresses lung tumor growth and controls differentiation. Cancer Discov. 9, 1590–1605. 10.1158/2159-8290.CD-18-1237. [PubMed: 31350327]
19. Faubert B, Vincent EE, Griss T, Samborska B, Izreig S, Svensson RU, Mamer OA, Avizonis D, Shackelford DB, Shaw RJ, and Jones RG (2014). Loss of the tumor suppressor LKB1 promotes metabolic reprogramming of cancer cells via HIF-1alpha. Proc. Natl. Acad. Sci. USA 111, 2554–2559. 10.1073/pnas.1312570111. [PubMed: 24550282]
20. Galan-Cobo A, Sitthideatphaiboon P, Qu X, Poteete A, Pisegna MA, Tong P, Chen PH, Boroughs LK, Rodriguez MLM, Zhang W, et al. (2019). LKB1 and KEAP1/NRF2 pathways cooperatively promote metabolic reprogramming with enhanced glutamine dependence in KRAS-mutant lung adenocarcinoma. Cancer Res. 79, 3251–3267. 10.1158/0008-5472.CAN-18-3527. [PubMed: 31040157]
21. Kottakis F, Nicolay BN, Roumane A, Karnik R, Gu H, Nagle JM, Boukhali M, Hayward MC, Li YY, Chen T, et al. (2016). LKB1 loss links serine metabolism to DNA methylation and tumorigenesis. Nature 539, 390–395. 10.1038/nature20132. [PubMed: 27799657]
22. Kim J, Hu Z, Cai L, Li K, Choi E, Faubert B, Bezwada D, Rodriguez-Canales J, Villalobos P, Lin YF, et al. (2017). CPS1 maintains pyrimidine pools and DNA synthesis in KRAS/LKB1-mutant lung cancer cells. Nature 546, 168–172. 10.1038/nature22359. [PubMed: 28538732]
23. Ullah MS., Davies AJ., and Halestrap AP. (2006). The plasma membrane lactate transporter MCT4, but not MCT1, is up-regulated by hypoxia through a HIF-1alpha-dependent mechanism. J. Biol. Chem. 281, 9030–9037. 10.1074/jbc.M511397200. [PubMed: 16452478]
24. Javaeed A, and Ghauri SK (2019). MCT4 has a potential to be used as a prognostic biomarker - a systematic review and meta-analysis. Onco Rev. 13, 403. 10.4081/oncol.2019.403.
25. Takenaga K, Koshikawa N, Akimoto M, Tatsumi Y, Lin J, Itami M, and Nagase H (2021). MCT4 is induced by metastasis-enhancing pathogenic mitochondrial NADH dehydrogenase gene mutations and can be a therapeutic target. Sci. Rep. 11, 13302. 10.1038/s41598-021-92772-1. [PubMed: 34172808]
26. Mookerjee SA, Gerencser AA, Nicholls DG, and Brand MD (2017). Quantifying intracellular rates of glycolytic and oxidative ATP production and consumption using extracellular flux measurements. J. Biol. Chem. 292, 7189–7207. 10.1074/jbc.M116.774471. [PubMed: 28270511]
27. Immunological Genome Project (2020). ImmGen at 15. Nat. Immunol. 21, 700–703. 10.1038/s41590-020-0687-4. [PubMed: 32577013]
28. Braun DA, Street K, Burke KP, Cookmeyer DL, Denize T, Pedersen CB, Gohil SH, Schindler N, Pomerance L, Hirsch L, et al. (2021). Progressive immune dysfunction with advancing disease stage in renal cell carcinoma. Cancer Cell 39, 632–648.e8. 10.1016/j.ccell.2021.02.013. [PubMed: 33711273]
29. Wang LX, Zhang SX, Wu HJ, Rong XL, and Guo J (2019). M2b macrophage polarization and its roles in diseases. J. Leukoc. Biol. 106, 345–358. 10.1002/JLB.3RU1018-378RR. [PubMed: 30576000]
30. Yao Y, Xu XH, and Jin L (2019). Macrophage polarization in physiological and pathological pregnancy. Front. Immunol. 10, 792. 10.3389/fimmu.2019.00792. [PubMed: 31037072]
31. Bianco C, and Mohr I (2019). Ribosome biogenesis restricts innate immune responses to virus infection and DNA. Elife 8, e49551. 10.7554/eLife.49551.
32. Nilsson MB, Langley RR, and Fidler IJ (2005). Interleukin-6, secreted by human ovarian carcinoma cells, is a potent proangiogenic cytokine. Cancer Res. 65, 10794–10800. 10.1158/0008-5472.CAN-05-0623. [PubMed: 16322225]

33. Mu X, Shi W, Xu Y, Xu C, Zhao T, Geng B, Yang J, Pan J, Hu S, Zhang C, et al. (2018). Tumor-derived lactate induces M2 macrophage polarization via the activation of the ERK/STAT3 signaling pathway in breast cancer. Cell Cycle 17, 428–438. 10.1080/15384101.2018.1444305. [PubMed: 29468929]
34. Kaushik DK, Bhattacharya A, Mirzaei R, Rawji KS, Ahn Y, Rho JM, and Yong VW (2019). Enhanced glycolytic metabolism supports transmigration of brain-infiltrating macrophages in multiple sclerosis. J. Clin. Invest. 129, 3277–3292. 10.1172/JCI124012. [PubMed: 31112527]
35. Errea A, Cayet D, Marchetti P, Tang C, Kluza J, Offermanns S, Sirard JC, and Rumbo M (2016). Lactate inhibits the pro-inflammatory response and metabolic reprogramming in murine macrophages in a GPR81-independent manner. PLoS One 11, e0163694. 10.1371/journal.pone.0163694.
36. Shen Z, Jiang L, Yuan Y, Deng T, Zheng YR, Zhao YY, Li WL, Wu JY, Gao JQ, Hu WW, et al. (2015). Inhibition of G protein-coupled receptor 81 (GPR81) protects against ischemic brain injury. CNS Neurosci. Ther. 21, 271–279. 10.1111/cns.12362. [PubMed: 25495836]
37. Gordon S (2016). Phagocytosis: an immunobiologic process. Immunity 44, 463–475. 10.1016/j.immuni.2016.02.026. [PubMed: 26982354]
38. Lawrence T, and Natoli G (2011). Transcriptional regulation of macrophage polarization: enabling diversity with identity. Nat. Rev. Immunol. 11, 750–761. 10.1038/nri3088. [PubMed: 22025054]
39. Poffenberger MC, Metcalfe-Roach A, Aguilar E, Chen J, Hsu BE, Wong AH, Johnson RM, Flynn B, Samborska B, Ma EH, et al. (2018). LKB1 deficiency in T cells promotes the development of gastrointestinal polyposis. Science 361, 406–411. 10.1126/science.aan3975. [PubMed: 30049881]
40. Haas R, Smith J, Rocher-Ros V, Nadkarni S, Montero-Melendez T, D'Acquisto F, Bland EJ, Bombardieri M, Pitzalis C, Perretti M, et al. (2015). Lactate regulates metabolic and pro-inflammatory circuits in control of T cell migration and effector functions. PLoS Biol. 13, e1002202. 10.1371/journal.pbio.1002202.
41. Waugh KA, Leach SM, Moore BL, Bruno TC, Buhrman JD, and Slansky JE (2016). Molecular profile of tumor-specific CD8+ T cell hypofunction in a transplantable murine cancer model. J. Immunol. 197, 1477–1488. 10.4049/jimmunol.1600589. [PubMed: 27371726]
42. Sanmamed MF, Nie X, Desai SS, Villaroel-Espindola F, Badri T, Zhao D, Kim AW, Ji L, Zhang T, Quinlan E, et al. (2021). A burned-out CD8+ T-cell subset expands in the tumor microenvironment and curbs cancer immunotherapy. Cancer Discov. 11, 1700–1715. 10.1158/2159-8290.CD-20-0962. [PubMed: 33658301]
43. Melero I, Hirschhorn-Cymerman D, Morales-Kastresana A, Sanmamed MF, and Wolchok JD (2013). Agonist antibodies to TNFR molecules that costimulate T and NK cells. Clin. Cancer Res. 19, 1044–1053. 10.1158/1078-0432.CCR-12-2065. [PubMed: 23460535]
44. Ward-Kavanagh LK, Lin WW, Sědý JR, and Ware CF (2016). The TNF receptor superfamily in Co-stimulating and Co-inhibitory responses. Immunity 44, 1005–1019. 10.1016/j.immuni.2016.04.019. [PubMed: 27192566]
45. Sade-Feldman M, Yizhak K, Bjorgaard SL, Ray JP, de Boer CG, Jenkins RW, Lieb DJ, Chen JH, Frederick DT, Barzily-Rokni M, et al. (2018). Defining T cell states associated with response to checkpoint immunotherapy in melanoma. Cell 175, 998–1013.e20. 10.1016/j.cell.2018.10.038. [PubMed: 30388456]
46. Wang B, Zhang W, Jankovic V, Golubov J, Poon P, Oswald EM, Gurer C, Wei J, Ramos I, Wu Q, et al. (2018). Combination cancer immunotherapy targeting PD-1 and GITR can rescue CD8(+) T cell dysfunction and maintain memory phenotype. Sci. Immunol. 3, eaat7061. 10.1126/sciimmunol.aat7061.
47. Newman AM, Steen CB, Liu CL, Gentles AJ, Chaudhuri AA, Scherer F, Khodadoust MS, Esfahani MS, Luca BA, Steiner D, et al. (2019). Determining cell type abundance and expression from bulk tissues with digital cytometry. Nat. Biotechnol. 37, 773–782. 10.1038/s41587-019-0114-2. [PubMed: 31061481]
48. Rittmeyer A, Barlesi F, Waterkamp D, Park K, Ciardiello F, von Pawel J, Gadgeel SM, Hida T, Kowalski DM, Dols MC, et al. (2017). Atezolizumab versus docetaxel in patients with previously treated non-small-cell lung cancer (OAK): a phase 3, open-label, multicentre randomised controlled trial. Lancet 389, 255–265. 10.1016/S0140-6736(16)32517-X. [PubMed: 27979383]

49. Garon EB, Rizvi NA, Hui R, Leighl N, Balmanoukian AS, Eder JP, Patnaik A, Aggarwal C, Gubens M, Horn L, et al. (2015). Pembrolizumab for the treatment of non-small-cell lung cancer. N. Engl. J. Med. 372, 2018–2028. 10.1056/NEJMoa1501824. [PubMed: 25891174]
50. Brahmer J, Reckamp KL, Baas P, Crinò L, Eberhardt WEE, Poddubskaya E, Antonia S, Pluzanski A, Vokes EE, Holgado E, et al. (2015). Nivolumab versus docetaxel in advanced squamous-cell non-small-cell lung cancer. N. Engl. J. Med. 373, 123–135. 10.1056/NEJMoa1504627. [PubMed: 26028407]
51. Carbone DP, Reck M, Paz-Ares L, Creelan B, Horn L, Steins M, Felip E, van den Heuvel MM, Ciuleanu TE, Badin F, et al. (2017). First-line nivolumab in stage IV or recurrent non-small-cell lung cancer. N. Engl. J. Med. 376, 2415–2426. 10.1056/NEJMoa1613493. [PubMed: 28636851]
52. Mok TSK, Wu YL, Kudaba I, Kowalski DM, Cho BC, Turna HZ, Castro G Jr., Srimuninnimit V, Laktionov KK, Bondarenko I, et al. (2019). Pembrolizumab versus chemotherapy for previously untreated, PD-L1-expressing, locally advanced or metastatic non-small-cell lung cancer (KEYNOTE-042): a randomised, open-label, controlled, phase 3 trial. Lancet 393, 1819–1830. 10.1016/S0140-6736(18)32409-7. [PubMed: 30955977]
53. Gainor JF, Shaw AT, Sequist LV, Fu X, Azzoli CG, Piotrowska Z, Huynh TG, Zhao L, Fulton L, Schultz KR, et al. (2016). EGFR mutations and ALK rearrangements are associated with low response rates to PD-1 pathway blockade in non-small cell lung cancer: a retrospective analysis. Clin. Cancer Res. 22, 4585–4593. 10.1158/1078-0432.CCR-15-3101. [PubMed: 27225694]
54. Ricciuti B, Arbour KC, Alessi JVM, Mahadevan N, Lindsay J, Sinha R, Vokes NI, Recondo G, Lamberti G, Rizvi H, et al. (2021). Association of a very high tumor mutational load with increased CD8+ and PD-1+ T-cell infiltration and improved clinical outcomes to PD-(L)1 blockade across different PD-L1 expression levels in non-small cell lung cancer. J. Clin. Oncol. 39, 9018. 10.1200/JCO.2021.39.15_suppl.9018.
55. Negrao MV, Skoulidis F, Montesion M, Schulze K, Bara I, Shen V, Xu H, Hu S, Sui D, Elamin YY, et al. (2021). Oncogene-specific differences in tumor mutational burden, PD-L1 expression, and outcomes from immunotherapy in non-small cell lung cancer. J. Immunother. Cancer 9, e002891. 10.1136/jitc-2021-002891.
56. Liu Y, Marks K, Cowley GS, Carretero J, Liu Q, Nieland TJF, Xu C, Cohoon TJ, Gao P, Zhang Y, et al. (2013). Metabolic and functional genomic studies identify deoxythymidylate kinase as a target in LKB1-mutant lung cancer. Cancer Discov. 3, 870–879. 10.1158/2159-8290.CD-13-0015. [PubMed: 23715154]
57. Dupuy F, Griss T, Blagih J, Bridon G, Avizonis D, Ling C, Dong Z, Siwak DR, Annis MG, Mills GB, et al. (2013). LKB1 is a central regulator of tumor initiation and pro-growth metabolism in ErbB2-mediated breast cancer. Cancer Metabol. 1, 18. 10.1186/2049-3002-1-18.
58. Faubert B, Boily G, Izreig S, Griss T, Samborska B, Dong Z, Dupuy F, Chambers C, Fuerth BJ, Viollet B, et al. (2013). AMPK is a negative regulator of the Warburg effect and suppresses tumor growth in vivo. Cell Metabol. 17, 113–124. 10.1016/j.cmet.2012.12.001.
59. Luo F, Zou Z, Liu X, Ling M, Wang Q, Wang Q, Lu L, Shi L, Liu Y, Liu Q, and Zhang A (2017). Enhanced glycolysis, regulated by HIF-1alpha via MCT-4, promotes inflammation in arsenite-induced carcinogenesis. Carcinogenesis 38, 615–626. 10.1093/carcin/bgx034. [PubMed: 28419250]
60. Walenta S, Wetterling M, Lehrke M, Schwickert G, Sundfør K, Rofstad EK, and Mueller-Klieser W (2000). High lactate levels predict likelihood of metastases, tumor recurrence, and restricted patient survival in human cervical cancers. Cancer Res. 60, 916–921. [PubMed: 10706105]
61. Qian J, Gong ZC, Zhang YN, Wu HH, Zhao J, Wang LT, Ye LJ, Liu D, Wang W, Kang X, et al. (2021). Lactic acid promotes metastatic niche formation in bone metastasis of colorectal cancer. Cell Commun. Signal. 19, 9. 10.1186/s12964-020-00667-x. [PubMed: 33478523]
62. Faubert B, Li KY, Cai L, Hensley CT, Kim J, Zacharias LG, Yang C, Do QN, Doucette S, Burguete D, et al. (2017). Lactate metabolism in human lung tumors. Cell 171, 358–371.e9. 10.1016/j.cell.2017.09.019. [PubMed: 28985563]
63. Tasdogan A, Faubert B, Ramesh V, Ubellacker JM, Shen B, Solmonson A, Murphy MM, Gu Z, Gu W, Martin M, et al. (2020). Metabolic heterogeneity confers differences in melanoma metastatic potential. Nature 577, 115–120. 10.1038/s41586-019-1847-2. [PubMed: 31853067]

64. Benjamin D, Robay D, Hindupur SK, Pohlmann J, Colombi M, El-Shemerly MY, Maira SM, Moroni C, Lane HA, and Hall MN (2018). Dual inhibition of the lactate transporters MCT1 and MCT4 is synthetic lethal with metformin due to NAD+ depletion in cancer cells. Cell Rep. 25, 3047–3058.e4. 10.1016/j.celrep.2018.11.043. [PubMed: 30540938]

65. Polański R, Hodgkinson CL, Fusi A, Nonaka D, Priest L, Kelly P, Trapani F, Bishop PW, White A, Critchlow SE, et al. (2014). Activity of the monocarboxylate transporter 1 inhibitor AZD3965 in small cell lung cancer. Clin. Cancer Res. 20, 926–937. 10.1158/1078-0432.CCR-13-2270. [PubMed: 24277449]

66. Latif A, Chadwick AL, Kitson SJ, Gregson HJ, Sivalingam VN, Bolton J, McVey RJ, Roberts SA, Marshall KM, Williams KJ, et al. (2017). Monocarboxylate Transporter 1 (MCT1) is an independent prognostic biomarker in endometrial cancer. BMC Clin. Pathol. 17, 27. 10.1186/s12907-017-0067-7. [PubMed: 29299023]

67. Leu M, Kitz J, Pilavakis Y, Hakroush S, Wolff HA, Canis M, Rieken S, and Schirmer MA (2021). Monocarboxylate transporter-1 (MCT1) protein expression in head and neck cancer affects clinical outcome. Sci. Rep. 11, 4578. 10.1038/s41598-021-84019-w. [PubMed: 33633176]

68. Payen VL, Hsu MY, Rädecke KS, Wyart E, Vazeille T, Bouzin C, Porporato PE, and Sonveaux P (2017). Monocarboxylate transporter MCT1 promotes tumor metastasis independently of its activity as a lactate transporter. Cancer Res. 77, 5591–5601. 10.1158/0008-5472.CAN-17-0764. [PubMed: 28827372]

69. Jang C, Lee G, and Chung J (2008). LKB1 induces apical trafficking of Silnoon, a monocarboxylate transporter, in Drosophila melanogaster. J. Cell Biol. 183, 11–17. 10.1083/jcb.200807052. [PubMed: 18838551]

70. Zhang W, Wang G, Xu ZG, Tu H, Hu F, Dai J, Chang Y, Chen Y, Lu Y, Zeng H, et al. (2019). Lactate is a natural suppressor of RLR signaling by targeting MAVS. Cell 178, 176–189.e15. 10.1016/j.cell.2019.05.003. [PubMed: 31155231]

71. Watson MJ, Vignali PDA, Mullett SJ, Overacre-Delgoffe AE, Peralta RM, Grebinoski S, Menk AV, Rittenhouse NL, DePeaux K, Whetstone RD, et al. (2021). Metabolic support of tumour-infiltrating regulatory T cells by lactic acid. Nature 591, 645–651. 10.1038/s41586-020-03045-2. [PubMed: 33589820]

72. de la Cruz-López KG, Castro-Muñoz LJ, Reyes-Hernández DO, García-Carrancá A, and Manzo-Merino J (2019). Lactate in the regulation of tumor microenvironment and therapeutic approaches. Front. Oncol. 9, 1143. 10.3389/fonc.2019.01143. [PubMed: 31737570]

73. Yang X, Lu Y, Hang J, Zhang J, Zhang T, Huo Y, Liu J, Lai S, Luo D, Wang L, et al. (2020). Lactate-modulated immunosuppression of myeloid-derived suppressor cells contributes to the radioresistance of pancreatic cancer. Cancer Immunol. Res. 8, 1440–1451. 10.1158/2326-6066.CIR-20-0111. [PubMed: 32917658]

74. Kumagai S, Koyama S, Itahashi K, Tanegashima T, Lin YT, Togashi Y, Kamada T, Irie T, Okumura G, Kono H, et al. (2022). Lactic acid promotes PD-1 expression in regulatory T cells in highly glycolytic tumor microenvironments. Cancer Cell 40, 201–218.e9. 10.1016/j.ccell.2022.01.001. [PubMed: 35090594]

75. Colegio OR, Chu NQ, Szabo AL, Chu T, Rhebergen AM, Jairam V, Cyrus N, Brokowski CE, Eisenbarth SC, Phillips GM, et al. (2014). Functional polarization of tumour-associated macrophages by tumour-derived lactic acid. Nature 513, 559–563. 10.1038/nature13490. [PubMed: 25043024]

76. Zhang D, Tang Z, Huang H, Zhou G, Cui C, Weng Y, Liu W, Kim S, Lee S, Perez-Neut M, et al. (2019). Metabolic regulation of gene expression by histone lactylation. Nature 574, 575–580. 10.1038/s41586-019-1678-1. [PubMed: 31645732]

77. Yang K, Xu J, Fan M, Tu F, Wang X, Ha T, Williams DL, and Li C (2020). Lactate suppresses macrophage pro-inflammatory response to LPS stimulation by inhibition of YAP and NF-kappaB activation via GPR81-mediated signaling. Front. Immunol. 11, 587913. 10.3389/fimmu.2020.587913.

78. Kitajima S, Ivanova E, Guo S, Yoshida R, Campisi M, Sundararaman SK, Tange S, Mitsuishi Y, Thai TC, Masuda S, et al. (2019). Suppression of STING associated with LKB1 loss in KRAS-driven lung cancer. Cancer Discov. 9, 34–45. 10.1158/2159-8290.CD-18-0689. [PubMed: 30297358]

79. Li R, Salehi-Rad R, Crosson W, Momcilovic M, Lim RJ, Ong SL, Huang ZL, Zhang T, Abascal J, Dumitras C, et al. (2021). Inhibition of granulocytic myeloid-derived suppressor cells overcomes resistance to immune checkpoint inhibition in LKB1-deficient non-small cell lung cancer. Cancer Res. 81, 3295–3308. 10.1158/0008-5472.CAN-20-3564. [PubMed: 33853830]
80. Mohammad Nezhady MA, and Chemtob S (2021). 3-OBA is not an antagonist of GPR81. Front. Pharmacol. 12, 803907. 10.3389/fphar.2021.803907.
81. Khatib-Massalha E., Bhattacharya S., Massalha H., Biram A., Golan K., Kollet O., Kumari A., Avemaria F., Petrovich-Kopitman E., Gur-Cohen S., et al. . (2020). Lactate released by inflammatory bone marrow neutrophils induces their mobilization via endothelial GPR81 signaling. Nat. Commun. 11, 3547. 10.1038/s41467-020-17402-2. [PubMed: 32669546]
82. Lee YS, Kim TY, Kim Y, Lee SH, Kim S, Kang SW, Yang JY, Baek IJ, Sung YH, Park YY, et al. (2018). Microbiota-derived lactate accelerates intestinal stem-cell-mediated epithelial development. Cell Host Microbe 24, 833–846.e6. 10.1016/j.chom.2018.11.002. [PubMed: 30543778]
83. Yang K, Fan M, Wang X, Xu J, Wang Y, Tu F, Gill PS, Ha T, Liu L, Williams DL, and Li C (2022). Lactate promotes macrophage HMGB1 lactylation, acetylation, and exosomal release in polymicrobial sepsis. Cell Death Differ. 29, 133–146. 10.1038/s41418-021-00841-9. [PubMed: 34363018]
84. Fang Y, Liu W, Tang Z, Ji X, Zhou Y, Song S, Tian M, Tao C, Huang R, Zhu G, et al. (2023). Monocarboxylate transporter 4 inhibition potentiates hepatocellular carcinoma immunotherapy through enhancing T cell infiltration and immune attack. Hepatology 77, 109–123. 10.1002/hep.32348. [PubMed: 35043976]
85. Stuart T, Butler A, Hoffman P, Hafemeister C, Papalexi E, Mauck WM 3rd, Hao Y, Stoeckius M, Smibert P, and Satija R (2019). Comprehensive integration of single-cell data. Cell 177, 1888–1902.e21. 10.1016/j.cell.2019.05.031. [PubMed: 31178118]
86. Trapnell C, Cacchiarelli D, Grimsby J, Pokharel P, Li S, Morse M, Lennon NJ, Livak KJ, Mikkelsen TS, and Rinn JL (2014). The dynamics and regulators of cell fate decisions are revealed by pseudotemporal ordering of single cells. Nat. Biotechnol. 32, 381–386. 10.1038/nbt.2859. [PubMed: 24658644]
87. Hänzelmann S, Castelo R, and Guinney J (2013). GSVA: gene set variation analysis for microarray and RNA-seq data. BMC Bioinf. 14, 7. 10.1186/1471-2105-14-7.
88. Roederer M, Nozzi JL, and Nason MC (2011). SPICE: exploration and analysis of post-cytometric complex multivariate datasets. Cytometry A. 79, 167–174. 10.1002/cyto.a.21015. [PubMed: 21265010]
89. Gentles AJ, Newman AM, Liu CL, Bratman SV, Feng W, Kim D, Nair VS, Xu Y, Khuong A, Hoang CD, et al. (2015). The prognostic landscape of genes and infiltrating immune cells across human cancers. Nat. Med. 21, 938–945. 10.1038/nm.3909. [PubMed: 26193342]
90. Xie Z, Bailey A, Kuleshov MV, Clarke DJB, Evangelista JE, Jenkins SL, Lachmann A, Wojciechowicz ML, Kropiwnicki E, Jagodnik KM, et al. (2021). Gene set knowledge discovery with enrichr. Curr. Protoc. 1, e90. 10.1002/cpz1.90. [PubMed: 33780170]
91. Li T, Fu J, Zeng Z, Cohen D, Li J, Chen Q, Li B, and Liu XS (2020). TIMER2.0 for analysis of tumor-infiltrating immune cells. Nucleic Acids Res. 48, W509–W514. 10.1093/nar/gkaa407. [PubMed: 32442275]
92. Le X, Negrao MV, Reuben A, Federico L, Diao L, McGrail D, Nilsson M, Robichaux J, Munoz IG, Patel S, et al. (2021). Characterization of the immune landscape of EGFR-mutant NSCLC identifies CD73/adenosine pathway as a potential therapeutic target. J. Thorac. Oncol. 16, 583–600. 10.1016/j.jtho.2020.12.010. [PubMed: 33388477]
93. Zhang X, Goncalves R, and Mosser DM (2008). The isolation and characterization of murine macrophages. Curr Protoc Immunol. Chapter 14. Unit 14 11. 10.1002/0471142735.im1401s83.
94. Wang R, Dang M, Harada K, Han G, Wang F, Pool Pizzi M, Zhao M, Tatlonghari G, Zhang S, Hao D, et al. (2021). Single-cell dissection of intratumoral heterogeneity and lineage diversity in metastatic gastric adenocarcinoma. Nat. Med. 27, 141–151. 10.1038/s41591-020-1125-8. [PubMed: 33398161]

Highlights

- *STK11*/LKB1 mutation is associated with increased MCT4 and lactate secretion
- MCT4-mediated lactate secretion polarizes M2 macrophage and suppresses T cell
- MCT4 depletion reverses the immunosuppressive phenotype mediated by LKB1 loss
- MCT4 depletion enhances sensitivity to immune checkpoint blockade

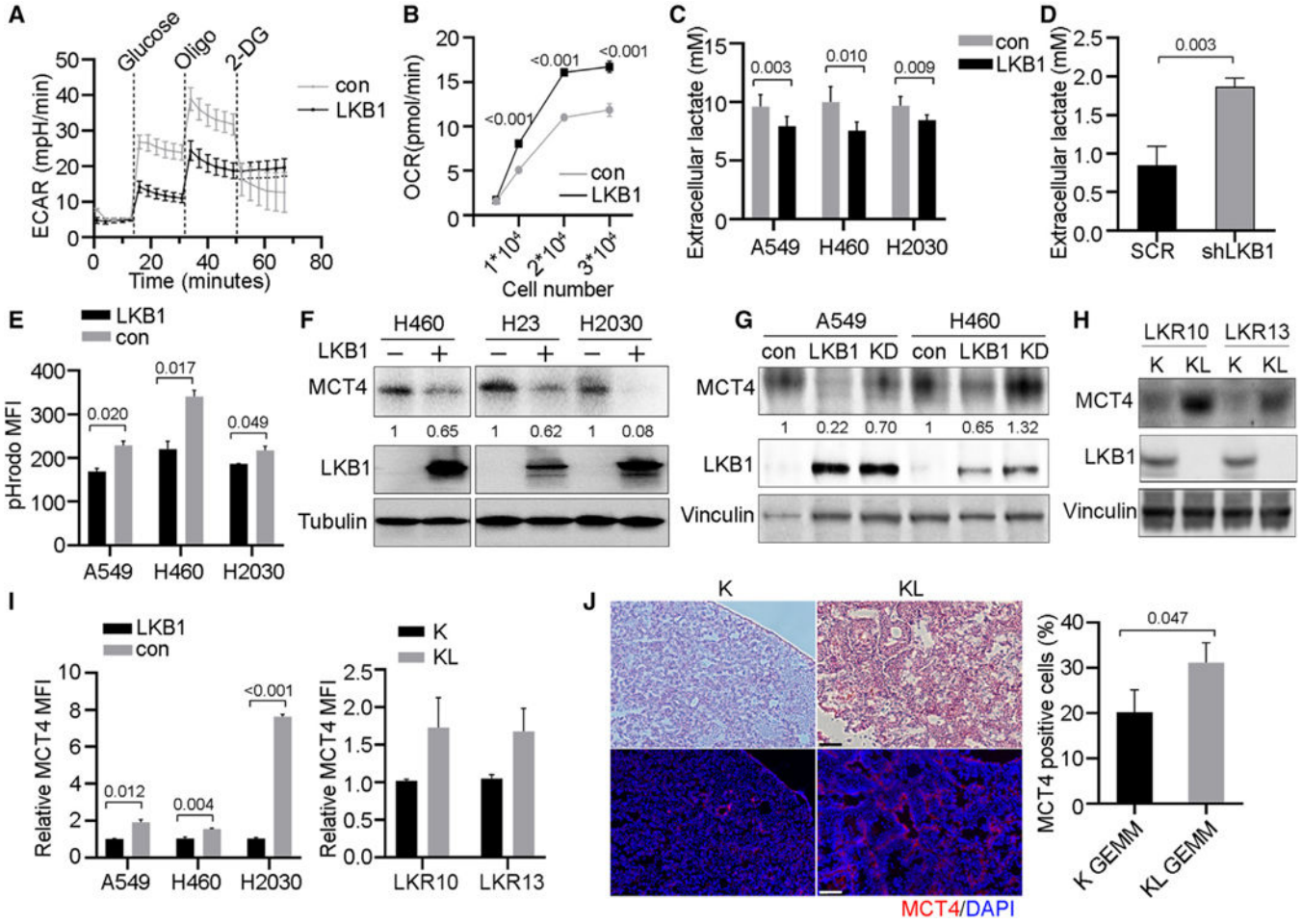

Figure 1. LKB1-deficiency induces metabolic alteration, increases glycolysis, lactate export, and MCT4 expression

(A) ECAR analysis of A549 con (LKB1-deficient) or LKB1 re-expression (LKB1-proficient) cells. Cells were detected at basal level, followed by adding glucose (10mM), oligomycin (Oligo, 1.5μM), and 2-DG (50mM). (n = 4).

(B) OCR analysis of A549 con and LKB1 cells. (n = 3).

(C) Extracellular lactate level of LKB1-proficient and deficient cell lines. (n = 6).

(D) Extracellular lactate level of H441 (LKB1-proficient) with or without LKB1 knockdown cells (n = 3).

(E) Intracellular pH level of LKB1-proficient and deficient cells. (n = 3).

(F) MCT4 expression was detected by Western blot in H460, H23, and H2030 cells with or without LKB1 overexpression. Numbers were the relative quantification of MCT4 bands and normalized to housekeeping gene.

(G) LKB1 kinase dead protein (LKB1 K78I, labeled as KD) was overexpressed in A549 and H460 cells. MCT4 expression was detected by Western blot. Numbers were the relative quantification of MCT4 bands and normalized to housekeeping gene.

(H) MCT4 expression in LKR10 and LKR13 K/KL cells.

(I) Cell surface staining of MCT4 was detected by flow cytometry in cells with or without LKB1. (n = 3).

(J) Immunofluorescence staining of MCT4 in K and KL GEMM models. Bar, 100μm. (n = 3). All quantitative data are represented as Mean ± SD; all statistical analysis (p values) are Student's *t* test.

See also Figure S1.

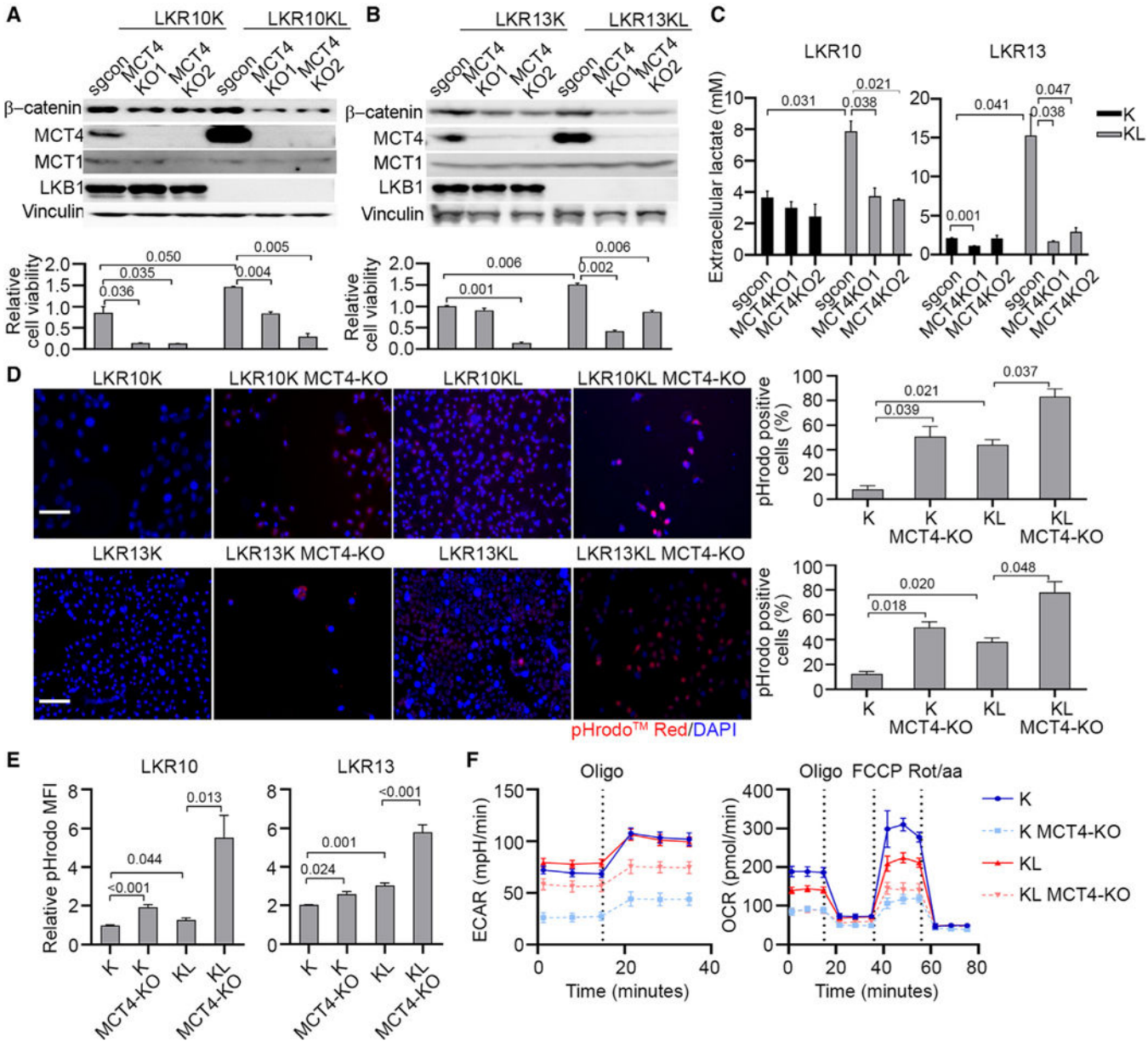

Figure 2. MCT4 knockout impairs lactate export and cell viability in LKB1 deficient cells

(A and B) Upper panel: Western blot confirms the MCT4 KO in K and KL cells in LKR10 cells (A) and LKR13 (B) models. Lower panel: statistical analysis of colony formation assay of K and KL cells with or without MCT4 KO. Representative data of triplicate experiments (n = 3).

(C) Extracellular lactate level of cells with MCT4 KO. Representative data of triplicate experiments (n = 3).

(D) Intracellular pH was detected by pHrodo Red, and representative images were shown in K and KL cells with MCT4 KO. Bar, 100μm. (n = 3).

(E) Intracellular pH was detected by flow cytometry. (n = 3–5).

(F) ECAR and OCR analysis of K and KL cells with MCT4 KO in LKR13 model. (n = 6). All quantitative data are represented as Mean ± SD; all statistical analysis are Student's *t* test.

See also Figure S2.

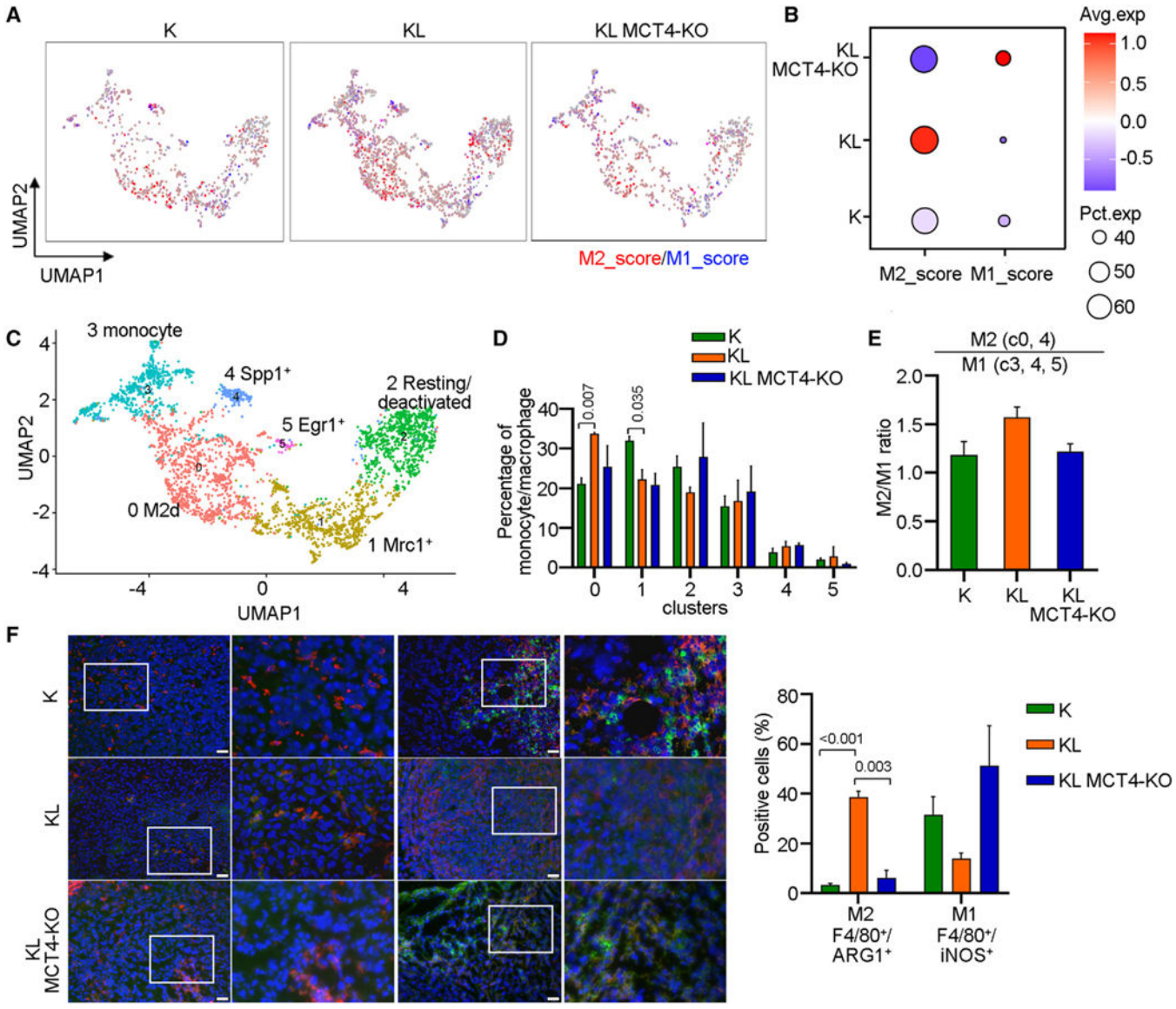

Figure 3. MCT4 knock-out abrogates M2 polarization induced in LKB1 deficient tumors

(A) UMAP plot of macrophage populations in K, KL, and KL MCT4-KO tumors highlighting M2-score and M1-scores.

(B) Dot plot of M2- and M1-scores in macrophages from three types of tumors.

(C) UMAP plot of macrophage clusters.

(D) The proportion of each macrophage sub-cluster from three types of tumors.

(E) M2-high cluster (c0, c4), M1-high cluster (c3, c4, c5), and the ratio.

(F) The presence of M2 macrophages ($F4/80^+ARG1^+$) and M1 macrophages ($F4/80^+iNOS^+$) was detected by immunofluorescence in K, KL, and KL MCT4-KO tumors (LKR13 model). Bar, 50μm. (n = 3–5). All quantitative data are represented as Mean ± SD; all statistical analysis are Student's *t* test.

See also Figure S3 and Table S1.

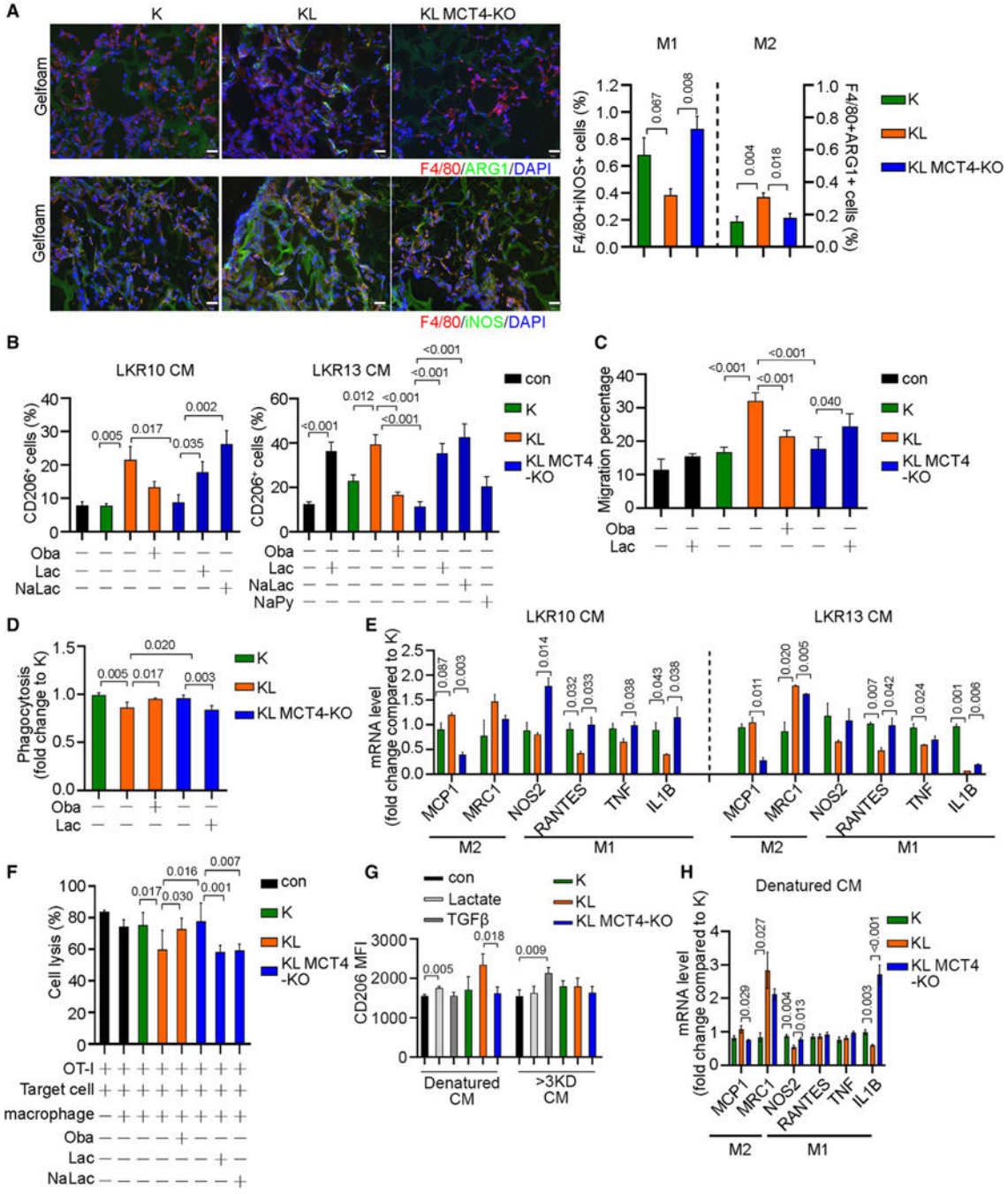

Figure 4. Targeting lactate secretion by MCT4 knockout decreases M2 macrophage polarization in LKB1 deficient tumor cells

(A)*In vivo* chemoattraction assay was performed using conditioned medium (CM) from K, KL, and KL MCT4-KO cells. Frozen slides were stained with M1, M2 markers, and representative images were shown. Bar, 50μm. (n = 4).

(B) $CD206^+$ M2-like cells were detected by flow cytometry after co-culturing Raw264.7 cells with CM from K, KL, and KL MCT4-KO tumor cells. Additional treatments were added as indicated. Oba, 3-hydroxy-butyrate (8mM); Lac, lactate (10mM); NaLac, sodium lactate (10mM); NaPy, sodium pyruvate (10mM). (n = 4–6).

(C) Cell migration assay of Raw264.7 cells co-cultured with CM and additional treatments. (n = 3–4).
(D) Phagocytosis analysis of Raw264.7 cells treated with CM from K, KL, and KL MCT4-KO tumor cells. Additional treatments were added as indicated. (n = 4).
(E) Representative markers of macrophage polarization were determined by qRT-PCR. (n = 4).
(F) Raw264.7 cells were treated with CM and then co-cultured with OT-I T cells and SIINFEKL-expressing cells. Cell lysis was measured. (n = 4–5).
(G) CM from K, KL, and KL MCT4-KO tumor cells either boiled to denature the bioactive protein or dialyzed by centrifuging to remove the metabolites. Raw264.7 cells were treated with denatured CM or filtered CM (>3KD CM). CD206 expression was detected by flow cytometry. Lactate (10mM) and TGF-β (20 ng/ml) were used as positive controls. (n = 3).
(H) M2 and M1 markers were detected in Raw264.7 cells treated with denatured CM. (n = 4). All quantitative data are represented as Mean ± SD; all statistical analysis are Student's *t* test.
See also Figure S4.

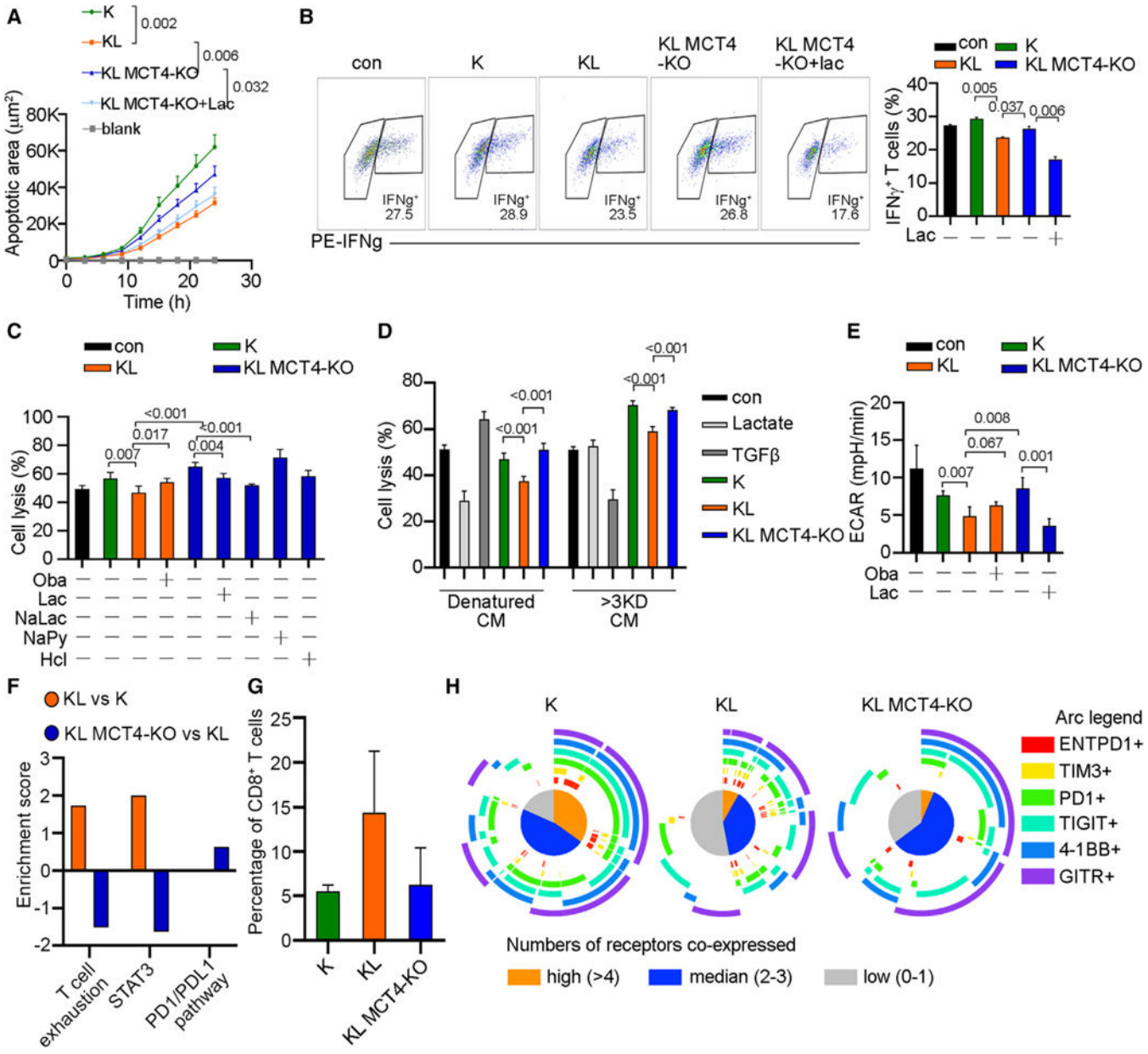

Figure 5. MCT4 knockout restores LKB1 deficiency induced CD8$^+$ T cell dysfunction

(A) CD8$^+$ T cells were isolated from OT-I mice and co-cultured with conditioned medium (CM) from K, KL, and KL MCT4-KO tumor cells, and performed targeted cell killing using LKR13K-SIINFEKL overexpressing cells. Cell apoptosis was monitored using Incucyte system. (n = 12).

(B) OT-I T cells were pre-treated with CM from K, KL, and KL MCT4-KO tumor cells, and then co-cultured with target cells for 6 h. T cells were collected and IFN-γ production was detected by flow cytometry (left). The statistical analysis of the IFN-γ$^+$ T cells according to the flow cytometry (right). (n = 4).

(C) OT-I T cells were co-cultured with indicated CM and additional treatments and targeted cell killing was performed. Hydrogen chloride was used as a low pH control. (n = 5).

(D) T cells were treated with denatured CM or filtered CM (>3KD CM) as in Figure 4G. Targeted cell killing was measured. (n = 6).
(E) ECAR analysis of OT-I T cells co-cultured with indicated CM and additional treatments. (n = 4).
(F) Ingenuity Pathway Analysis (IPA) of differential expressed genes in $CD8^+$ T cells comparing KL with K tumors, or KL MCT4-KO with KL tumors, respectively, based on scRNA-seq data.
(G) The proportion of hypofunctional T cells in three types of tumors.
(H) Immune checkpoint markers and co-stimulator co-expression in the $CD8^+$ T cells from three types of tumors. All quantitative data are represented as Mean ± SD; all statistical analysis are Student's *t* test.
See also Figure S5 and Table S2.

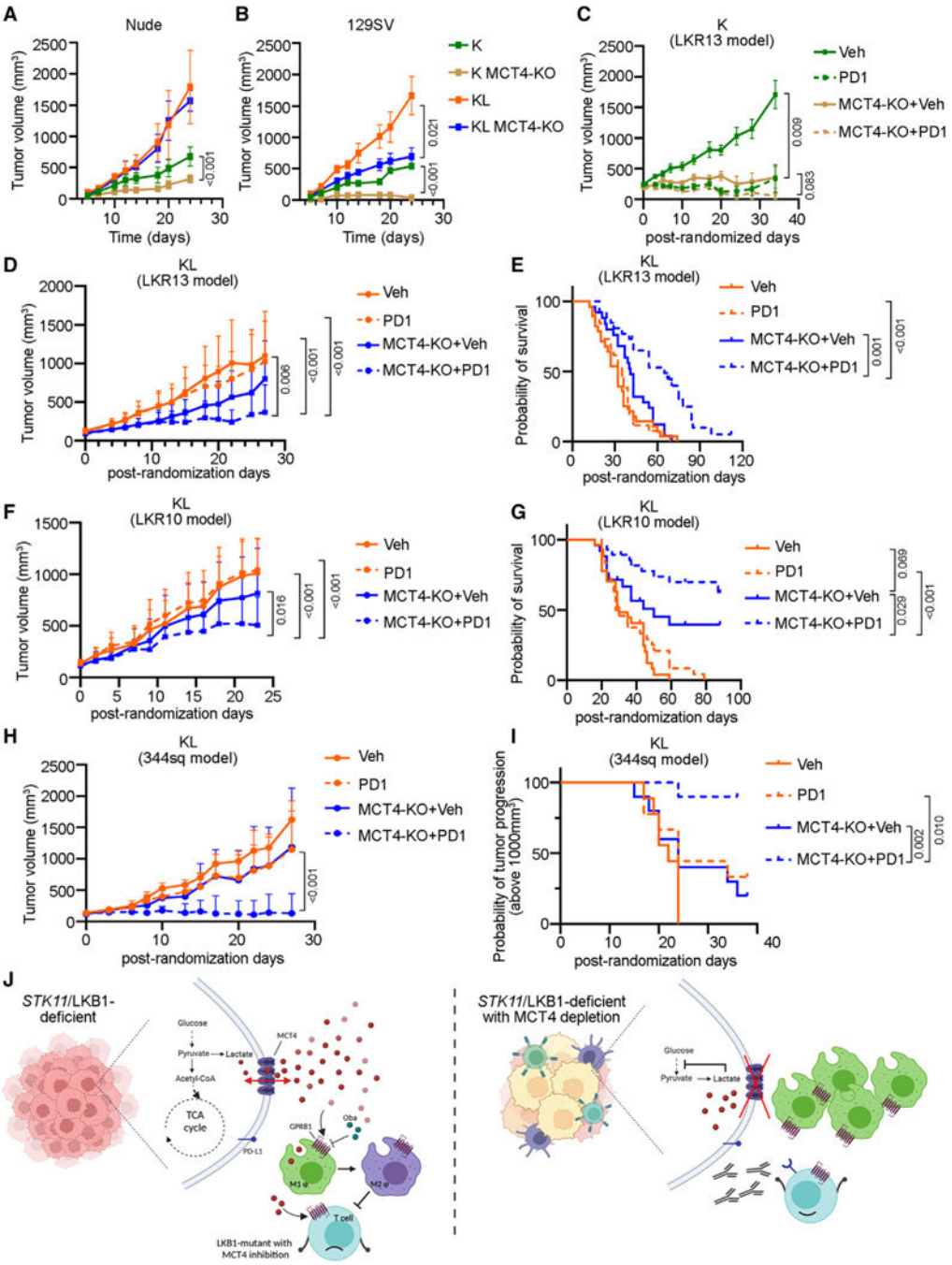

Figure 6. MCT4 knockout impairs tumor growth and enhances immunotherapy response in LKB1 deficient tumors

(A and B) LKR13K and LKR13KL cells with or without MCT4 KO were injected in immunodeficient mice (nude, A), and immunocompetent mice (129SV, B). Tumor growth was monitored. (n = 6–7).

(C) Syngeneic model was performed by subcutaneously injecting LKR13K cells with or without MCT4 expression into the flank of 129SV mice. Once tumors reached 150–250 mm^3, animals were randomized to receive anti-PD-1 or IgG control. Tumor growth was monitored. (n = 6–10).

(D) Tumor growth of LKR13KL with or without MCT4 KO tumors treated with IgG or anti-PD1. (n = 16–18).
(E) Kaplan-Meier curve of LKR13KL with or without MCT4 KO treated with IgG or anti-PD1. (n = 16–18).
(F and G) Tumor growth (F) and survival analysis (G) from LKR10KL model. (n = 16–18).
(H and I) Tumor growth (H) and tumor progression (cutoff tumor volume > 1000mm,^{3} I) of 344sq LKB1 KO cells with or without MCT4 KO and treated with IgG or anti-PD1. (n = 10).
(J) Schematic of MCT4 impact on regulating TME. All quantitative data are represented as Mean ± SD; Student's *t* test used for comparing groups at the last time point, A, B, C, D, F, H; Log rank test, E, G, I.
See also Figure S6.

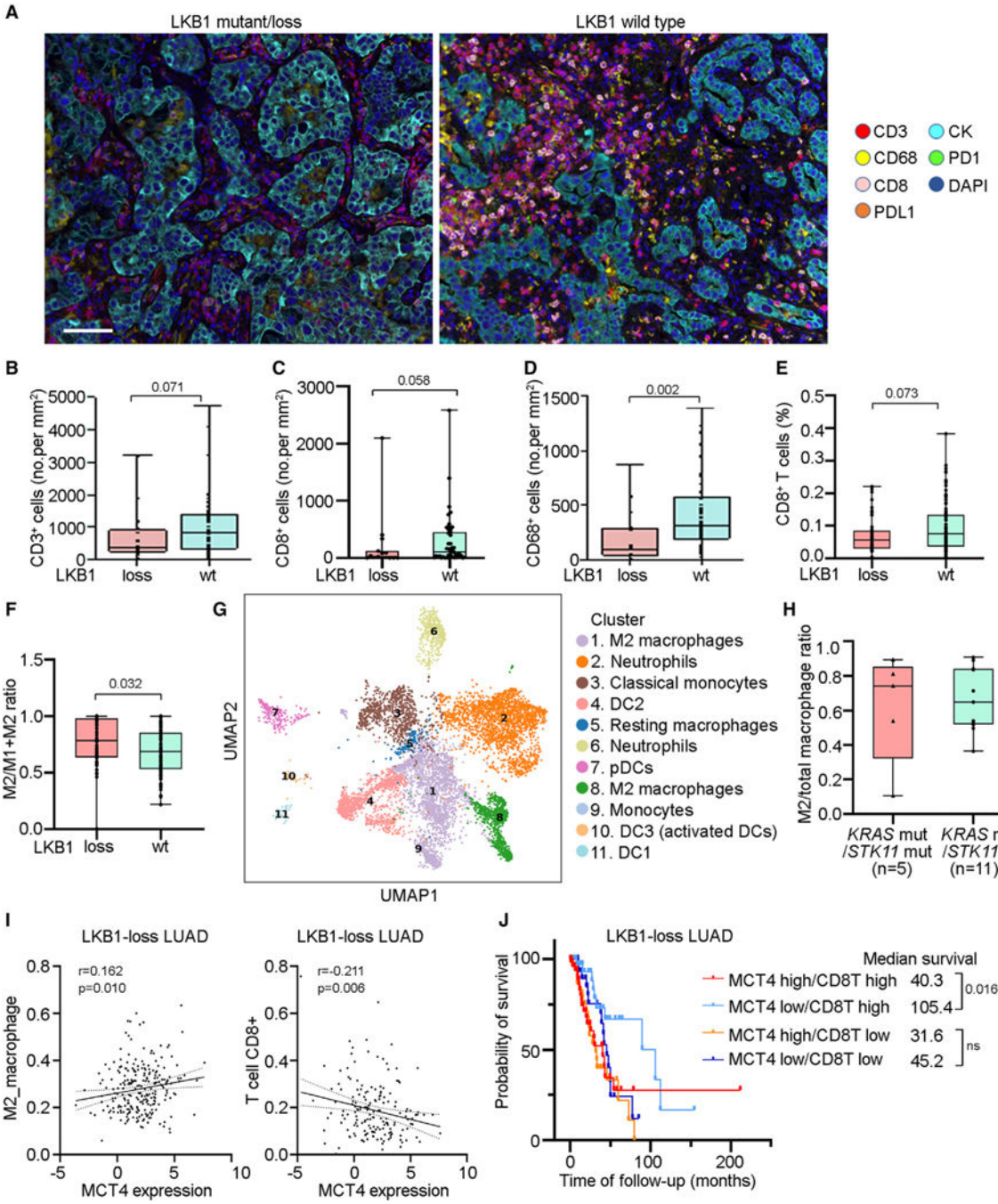

Figure 7. LKB1 loss is associated with reduced T cells tumor infiltration and M2 polarization in LUAD patients

(A) Representative image of multiplex IHC (mIHC) in LKB1-deficient (mutant/loss) and wild-type (WT) LUAD tumors from MDACC ICON dataset. Bar, 100μm.

(B–D) The presence of $CD3^+$ (B) and $CD8^+$ (C) and $CD68^+$ (D) cells in LKB1-deficient and WT NSCLC tissues.

(E) CIBERSORT analysis was performed in PROSPECT cohort to estimate the immune cell infiltration. The abundance of $CD8^+$ T cells in LKB1-deficient and WT tumors was shown.

(F) M2 macrophage ratio was compared in LKB1-deficient and WT tumors based on CIBERSORT analysis.
(G) The UMAP plot of the myeloid cell population clusters in Massachusetts General Hospital (MGH)'s patient cohort.
(H) The ratio of M2 macrophages in all macrophage populations according to the mutation status.
(I) The correlation between M2 macrophage infiltration, $CD8^+$ T cell infiltration and MCT4 expression in LKB1-mutant LUAD TCGA cohort.
(J) The patients from LKB1-mutant LUAD TCGA cohort were sub-grouped by MCT4 expression and $CD8^+$ T infiltration. The Kaplan-Meier curves were shown.
Data are represented as boxplot (B, C, D, E, F, H, top line, third quartile, middle line, median, bottom line, first quartile, whiskers, minimum and maximum data points). Mann-Whitney test, B, C, D, E, F; Pearson correlation coefficient, I; Log rank test, J.
See also Figure S7.

KEY RESOURCES TABLE

REAGENT or RESOURCE	SOURCE	IDENTIFIER
Antibodies		
LKB1 (D60C5) Rabbit mAb	CST	#3047; RRID: AB_2198327
MCT4 Antibody (D-1)	Santa Cruz Bio	sc-376140; RRID: AB_10992036
Anti-Monocarboxylate Transporter 4 Antibody	Milllipore	AB3314P, RRID: AB_2286063
MCT1 Monoclonal Antibody	Invitrogen	P14612; RRID: AB_2539662
Anti-β-catenin	Upstates Biotechnology	05–482
Phospho-p44/42 MAPK (Erk1/2) (Thr202/Tyr204) (E10) Mouse mAb	CST	#9106; RRID: AB_331768
p44/42 MAPK (Erk1/2) Antibody	CST	#9102; RRID: AB_330744
Phospho-Stat1 (Tyr701) (58D6) Rabbit mAb	CST	#9167; RRID: AB_10860071
Monoclonal Anti-Vinculin antibody	Sigma	V9131; RRID: AB_477629
Monoclonal Anti-β-Actin antibody	Sigma	A5441; RRID: AB_476744
β-Tubulin (D3U1W) Mouse mAb	CST	#86298, RRID: AB_2715541
Anti-F4/80 antibody [CI:A3–1]	Abcam	ab6640; RRID: AB_1140040
Brilliant Violet 421™ anti-mouse/human CD11b	BioLegend	101236; RRID: AB_11203704
FITC anti-mouse CD11c	BioLegend	117306; RRID: AB_313775
PerCP anti-mouse CD8a	BioLegend	100732; RRID: AB_893423
PerCP/Cyanine5.5 anti-mouse TNF-α [Clone: MP6-XT22]	BioLegend	506322, RRID: AB_961434
PE anti-mouse IFN-γ [Clone: XMG1.2]	BioLegend	505808, RRID: AB_315402
APC anti-mouse F4/80 Antibody	BioLegend	123116; RRID: AB_893481
Brilliant Violet 711™ anti-mouse CD206 (MMR) Antibody	BioLegend	141727, RRID: AB_2565822
PE anti-mouse CD206 (MMR) Antibody	BioLegend	141706, RRID: AB_10895754
PE anti-mouse CD279 (PD-1)	BioLegend	135206, RRID: AB_1877231
PE anti-mouse CD274 (B7-H1)	eBioscience	12–5982-83, RRID: AB_466090
iNOS Monoclonal Antibody (4E5)	ThermoFisher	MA5–17139; RRID: AB_2538610
Arginase-1 (D4E3M™) XP® Rabbit mAb	CST	#93668; RRID: AB_2800207
Goat anti-Rabbit IgG (H+L) Cross-Adsorbed Secondary Antibody, Alexa Fluor 488	Invitrogen	A11008; RRID: AB_143165
Goat anti-Mouse IgG (H+L) Highly Cross-Adsorbed Secondary Antibody, Alexa Fluor 488	Invitrogen	A11029; RRID: AB_138404
Goat anti-Rat IgG (H+L) Cross-Adsorbed Secondary Antibody, Alexa Fluor 594	Invitrogen	A11007; RRID: AB_10561522
Goat Anti-Mouse IgG (H + L)-HRP Conjugate	Bio-rad	1706516; RRID: AB_11125547

REAGENT or RESOURCE	SOURCE	IDENTIFIER
Goat Anti-Rabbit IgG (H + L)-HRP Conjugate	Bio-rad	1706515; RRID: AB_11125142
Chemicals, peptides, and recombinant proteins		
anti-PD-1	Bio X Cell	#BE0146
isotype control IgG	Bio X Cell	#BE0089
InVivoMab anti-mouse CD8, Clone 2.43	Bio X Cell	#BE0061
Lipofectamine™ 2000 Transfection Reagent	Invitrogen	11668027
Puromycin	Invitrogen	A1113803
Cell Lysis Buffer (10X)	CST	#9803
PhosStop, 20 Tablets	Fisher Scientific	501003268
Complete protease inhibitor tablets	Fisher Scientific	501003279
Crystal Violet	Sigma	C6158
Fixation buffer	BioLegend	420801
Perm Wash Buffer	BioLegend	421002
Cell staining Buffer	BioLegend	421201
pHrodo™ Red AM Intracellular pH Indicator	Invitrogen	P35372
MitoTracker™ Deep Red FM	Invitrogen	M22426
Incucyte® Caspase-3/7 Green Dye for Apoptosis	Essen Bioscience Inc	4440
VECTASHIELD® Antifade Mounting Medium with DAPI	Vector Laboratories	H-1200–10
Collagenase A	Sigma	11088793001
Hyaluronidase	Sigma	H3506–500MG
DNase I	Sigma	D4513–1VL
Dispase	Stemcell	07913
Brewer thioglycollate medium	Sigma	B2551–500G
Matrigel matrix	Coming	356237
GELFOAM Sterile Sponge	Pfizer	09–0353-01
anti-mouse CD28, clone 37.51	Bio X Cell	BE0015–1
anti-mouse CD3ε, clone 145–2C11	Bio X Cell	BE0001–1
Murine IL-2	R&D Syetems	402-ML-020
Murine IL-7	R&D Syetems	407-ML-005
Recombinant Human TGF-β1	PeproTech	P01137

REAGENT or RESOURCE	SOURCE	IDENTIFIER
ITS	ThermoFisher	51300044
D-Luciferin	Fisher Scientific	501532814
2-mercaptoethanol	ThermoFisher	21985023
L-(+)-Lactic acid	Sigma	L6402–10G
(±)-Sodium 3-hydroxybutyrate	Sigma	54965–10G-F
AICAR	Selleck Chemicals	S1802
Compensation Beads	BioLegend	424602
Sodium pyruvate powder	Sigma	P5280
Sodium L-lactate	Sigma	71718
Critical commercial assays		
RNeasy Plus Mini Kit	Qiagen	74136
QIAprep Spin Miniprep Kit	Qiagen	27106
SuperScript™ III First-Strand Synthesis System	ThermoFisher	18080051
PerfeCTa SYBR Green FastMix Low ROX	QuantaBio	95074–012
Pierce™ BCA Protein Assay Reagent B	ThermoFisher	23224
SuperSignal™ West Pico PLUS Chemiluminescent Substrate	ThermoFisher	34580
L-Lactate Assay	ScienCell	8308
Lactate-Glo™ Assay kit	Promega	J5022
Glucose-Glo™ Assay	Promega	J6021
EasySep™ Mouse $CD8^+$ T Cell Isolation Kit	StemCell	#19854
Seahorse XF Cell Mito Stress Test Kit	Agilent	103015–100
MycoAlert™ Mycoplasma Detection Kit	Lonza	LT07–318
ELISA MAX™ Standard Set Mouse IFN-γ	BioLegend	430801
CellTrace™ CFSE Cell Proliferation Kit	Invitrogen	C34554
Experimental models: Cell lines		
Human: A549 con/LKB1 isogeneic pair	Lab preserve	
Human: H460 con/LKB1 isogeneic pair	Lab preserve	
Human: H2030 con/LKB1 isogeneic pair	Lab preserve	
Human: H23 con/LKB1 isogeneic pair	Lab perserve	

REAGENT or RESOURCE	SOURCE	IDENTIFIER
Human: HEK293T, H358, H441, H2009, H1792, H2122, HCC44, H1355, H1944	Lab preserve	
Mouse: LKR10K, LKR10KL, LKR13K, LKR13KL, 344sq	Lab preserve	
Mouse: Raw264.7	Lab preserve	
Phoenix cells	Lab perserve	
Experimental models: Organisms/strains		
Mouse: C56BL/6	Lab preserve	
Mouse: 129sv	Lab preserve	
Mouse: OT-I	Jackson Laboratory	
Mouse: $Kras^{G12D}$ GEM	Lab preserve	
Mouse: $Kras^{G12D}$; $Stk11^{fl/fl}$ GEM	Lab preserve	
Mouse: Nude	Lab preserve	
Oligonucleotides		
Primers for qPCR,	This paper	see Table S3
Recombinant DNA		
MCT4 CRISPR/Cas9 plasmid	Santa Cruz Bio	sc-429828
LKB1 CRISPR/Cas9 KO plasmid (h)	Santa Cruz Bio	sc-400313
LKB1 CRISPR/Cas9 KO Plasmid (m)	Santa Cruz Bio	sc-423192
pBABE-FLAG-KD LKB1	Addgene	#8593
pHIV-Luc-ZsGreen	Addgene	#39196
psPAX2	Addgene	#12260
pMD2.G	Addgene	#12259
Software and algorithms		
Fiji/Image J		https://imagej.net/Fiji
FlowJo v10	FlowJo, LLC	RRID: SCR 008520
Wave	Agilent	RRID: SCR_014526
R	CRAN	https://www.r-project.org/
Python		https://www.python.org/

REAGENT or RESOURCE	SOURCE	IDENTIFIER
Seurat	Stuart et al., [85]	https://satijalab.org/seurat/
Monocle 2	Trapnell et al., [86]	http://cole-trapnell-lab.github.io/monocle-release/
GSVA	Hanzelmann et al., [87]	https://bioconductor.org/packages/release/bioc/html/GSVA.html
Ingenuity Pathway Analysis	Qiagen	RRID: SCR_008653
SPICE	Roederer et al., 2011[88]	https://niaid.github.io/spice/; RRID: SCR 016603
CIBERSORTx	Newman et al., [47]	https://cibersortx.stanford.edu/
GraphPad Prism 8	GraphPad Prism	https://www.graphpad.com/scientific-software/prism/
PRECOG	Gentles et al., 2[89]	https://precog.stanford.edu/
Enrichr	Xie et al., [90]	https://maayanlab.doud/Enrichr/
TIMER 2.0	Li et al., [91]	http://timer.cistrome.org/
Other		
ABI7500 FAST real-time PCR system	ThermoFisher	
BD FACSCanto II system	BD	
Seahorse eXF96 system	Agilent	
Transwell chamber	Corning	354578
Amicon« Ultra-4 Centrifugal Filter Unit	EMD Millipore Corporation	UFC800324
Live-Cell Analysis Instruments	SARTORIUS	